Decays of the $\psi(3097)$ to baryon-antibaryon final states

M. W. Eaton,[a] G. Goldhaber, G. S. Abrams, C. A. Blocker,[a]
W. C. Carithers, W. Chinowsky, M. W. Coles,[b] S. Cooper,[c]
W. E. Dieterle, J. B. Dillon,[d] G. Gidal, A. D. Johnson, J. A. Kadyk,
A. J. Lankford, M. Levi,[a] R. E. Millikan, M. E. Nelson, C. Y. Pang,
J. F. Patrick,[e] J. Strait,[f] G. H. Trilling, E. Vella,[g] and I. Videau,[h]
Lawrence Berkeley Laboratory and Department of Physics, University of California, Berkeley, California 94720

M. S. Alam,[i] A. M. Boyarski, M. Breidenbach, D. L. Burke,
J. Dorenbosch,[g] J. M. Dorfan, G. J. Feldman, M. E. B. Franklin,
G. Hanson, K. G. Hayes, T. Himel,[g] D. G. Hitlin,[j]
R. J. Hollebeek, W. R. Innes, J. A. Jaros, P. Jenni,[g] R. R. Larsen,
V. Lüth, M. L. Perl, B. Richter, A. Roussarie,[k] D. L. Scharre,
R. H. Schindler,[j] R. F. Schwitters,[a] J. L. Siegrist, H. Taureg,[g]
M. Tonutti,[l] R. A. Vidal,[e] J. M. Weiss,[m] and H. Zaccone,[h]
Stanford Linear Accelerator Center, Stanford University, Stanford, California 94305

(Received 3 October 1983)

A high-statistics study of ψ decays into baryon final states has been done with the Mark II detector at SPEAR. A detailed test of baryon-antibaryon decay modes is presented. Substantial resonance formation is observed in multibody decays of the ψ involving baryons. Branching ratios for a large number of decay modes are given, including the radiative decay $\psi\to p\bar{p}\gamma$. The flavor-SU(3)-forbidden decays $\psi\to\Sigma^{\pm}(1385)\bar{\Sigma}^{\mp}$ + charge conjugate are observed with substantial branching ratios.

I. INTRODUCTION

We begin with a discussion of the implications of the flavor-SU(3) [$SU(3)_f$] content of the $\psi(3097)$ for exclusive final states. Due to the large mass difference between the charmed quark and the up, down, and strange quarks, the ψ is expected to be predominantly a pure charmonium state, with very little mixing of lighter quarks. Thus the ψ should be almost a pure $SU(3)_f$ singlet, and its decay amplitude into baryon-antibaryon final states of the same $SU(3)_f$ structure should be the same, except for phase-space considerations. In addition, the decay amplitude for nonsinglet baryon-antibaryon final states should be strongly suppressed relative to singlet final states.

Substantial branching ratios for direct photon decays of the ψ are a prediction[1-10] of QCD. A substantial fraction of the predicted direct photon contribution is accounted for by exclusive decays of the ψ, such as $\gamma\eta$, $\gamma\eta'$, $\gamma f^0(1270)$, and the recently observed[11,12] $\gamma\iota(1420)$ or $\gamma E(1420)$ and $\gamma\theta(1640)$. The ratio of the inclusive direct-photon width to the hadronic width is calculable[13,14] to first order in QCD. The predicted (and observed)[15-17] feature is that the direct-photon width is suppressed by only about an order of magnitude relative to the hadronic width.

This paper is organized as follows. The Introduction is followed by a discussion of the apparatus. Track and vertex selection is discussed in Sec. III, followed by a discussion of the Monte Carlo simulation, used for acceptance calculations, as well as the normalization calculation. Section V discusses decays of the type[18] $\psi\to B_8\bar{B}_8$, while Sec. VI discusses decays of the type $\psi\to B_{10}\bar{B}_{10}$. We find excellent agreement with the flavor independence of the ψ decay to baryon-antibaryon. Section VII discusses decays of the type[19] $\psi\to B_8\bar{B}_{10}$. The clear evidence for these types of $SU_f(3)$-forbidden decays is surprising in light of the results of the previous two sections. Section VIII discusses radiative decays of the ψ, while Sec. IX discusses a large variety of three-body decay modes of the ψ. Multibody decay modes of the ψ are discussed in Sec. X, while Sec. XI summarizes the results of this paper.

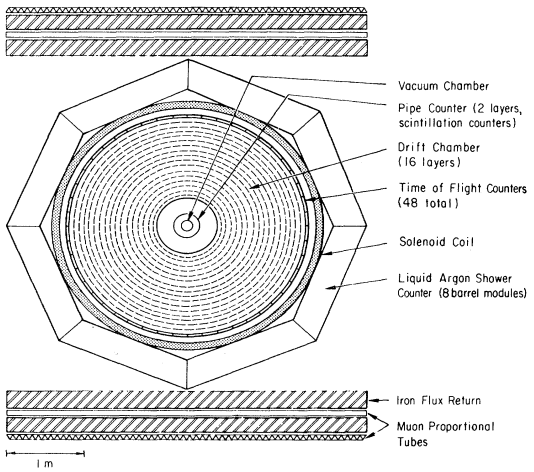

FIG. 1. Mark II detector (beam-line view). Detector components are shown in figure.

II. THE MARK II APPARATUS

The Mark II apparatus, as configured for SPEAR operation, has been fully discussed[20] elsewhere, and will only be recalled briefly here. Figure 1 shows the detector from a beam-line view. Charged particles are detected over 85% of 4π sr by 16 cyclindrical layers of drift chamber immersed in a uniform 4.16-kG magnetic field. The momentum resolution σ_p for tracks constrained to pass through the beam-beam interaction point (IP) is

$$\frac{\sigma_p}{p}=[(0.015)^2+(0.007p)^2]^{1/2}\,, \tag{1}$$

where p is the momentum in GeV/c.

Outside the drift chambers is a cyclindrical array of 48 time-of-flight (TOF) scintillation counters covering 75% of 4π sr, having 300-ps resolution for hadrons. Outside the TOF system is the aluminum magnet coil of 1.36 radiation lengths, followed by eight lead—liquid-argon (LA) shower-counter modules covering 65% of 4π sr, with an energy resolution of $12\%/\sqrt{E}$, where E is in GeV.

The Mark II is triggered by one or more charged particles identified by hardware track processors[21] which take information from selected drift-chamber layers and the TOF system to form track candidates. For the decay modes considered here, the trigger efficiency is[22] $>99.7\%$.

III. TRACK AND VERTEX SELECTION

For decay modes which do not involve weakly decaying particles, we require the charged particles to come within 1.5 cm in the transverse direction and 8 cm in the longitudinal direction with respect to the IP. To improve momentum resolution, charged tracks are constrained to the IP. Such a charged track is called a prong.

Charged particles are identified by the TOF system. A normalized weight

$$W(m)=\frac{1}{N}\exp\left[\frac{[t_m-t_p(m)]^2}{2\sigma^2}\right], \tag{2}$$

where t_m is the measured flight time, $t_p(m)$ is the predicted flight time for mass hypothesis m, σ is the TOF resolution, and N is the sum of the weights, is calculated[23] for each of the π, K, and p mass hypotheses. Track assignments are based on the highest weight of the three. In case of inconsistent or missing TOF information, the assignment defaults to a pion. The TOF resolution separates protons from kaons at the several-standard-deviation level for momenta less than 1.2 GeV/c.

The Λ is detected by its $p\pi^-$ decay mode, and is selected by cuts on the decay vertex. The decay vertex is required to lie within 1.5 cm transversely from the line defined by the Λ momentum vector and the IP. In addition, the decay length must be more than -5 cm from the IP, where the sign of the decay length is determined by the Λ direction. This allows for Λ decays very near the IP. These loose cuts dramatically decrease the beam-gas contamination while eliminating few real Λ events. A cut of $1.110<m(\Lambda)<1.122$ GeV/c^2 on the $p\pi^-$ mass is applied, and the decay products are constrained to the decay vertex to improve momentum resolution. Figure 2 shows the resultant $p\pi^-$ mass spectrum after vertex cuts.

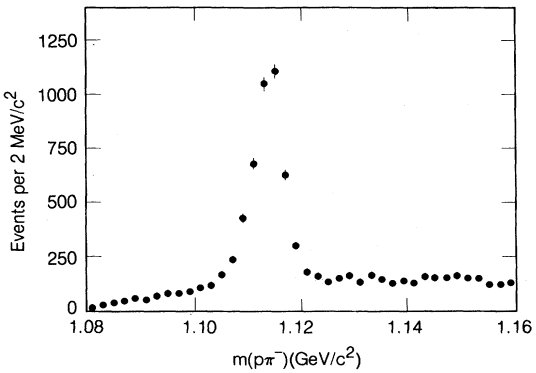

FIG. 2. $m(p\pi^-)$ for all pairs after vertex selection, showing the Λ signal. Note that the charge-conjugate mode is not included in this plot.

Photons are reconstructed in the LA shower counters. Corrections are made in software for correlated detector noise which may produce false photons. This analysis uses only the reconstructed photon direction but not the measured energy. The detection efficiency for photons in the LA fiducial volume is $>95\%$ for photon energy $E_\gamma>600$ MeV, but falls to zero near $E_\gamma=100$ MeV due to interactions in the magnet coil, electronics noise, and depth segmentation.

IV. MONTE CARLO SIMULATION AND NORMALIZATION

The detection efficiency for exclusive final states is estimated via a Monte Carlo simulation of detector performance. The detector simulation has been discussed elsewhere[24] and we discuss here only the physical assumptions contained within the Monte Carlo generator.

All Monte Carlo simulations assume a uniform phase-space distribution, and systematic errors in this assumption are separately estimated for each decay mode based on the acceptance and the actual data distributions. These systematic uncertainties are included in the quoted systematic error for each decay mode.

Detailed checks have been made[25] on the simulation program for possible systematic biases in the efficiencies estimated by the program. The biases encountered are almost always small compared to the statistical error from the data distributions used in the checks, which ranges from 2.7 to 8.4% depending on the check performed. As a result, the errors from these checks are added in quadrature with other systematic errors as a measure of the uncertainty between the simulation and the actual detector performance.

All of the branching-ratio calculations in this paper are of the form

$$B(\psi\to X)=\frac{N(X)}{\epsilon N(\psi)}\,, \tag{3}$$

where $N(X)$ is the observed number of events, $N(\psi)$ is the

TABLE I. Summary of produced ψ by run cycle.

Run cycles 1 and 2	6.57×10^5
Run cycles 3 (no LA system)	6.64×10^5
Total	1.32×10^6

number of produced ψ's, and ϵ is the detection efficiency. For brevity, we shall simply quote the result of such a calculation in the text and in Table VI. The details are fully discussed elsewhere.[25]

The number of produced ψ is calculated by knowing the trigger efficiency for ψ decays. The trigger efficiency calculation has been fully discussed in Ref. 16. It relies on the fact that the charged pions from the decay

$$\psi' \to \pi^+\pi^-\psi \,, \tag{4}$$

may satisfy the trigger requirements and thus the trigger information for the ψ decay products may be investigated. This information is used to determine the number of produced ψ in the data sample. Table I summarizes the results of these calculations.

The final quoted systematic error for the measurements presented here has folded in quadrature the statistical errors from the bias checks, the error in the normalization calculation, and either an estimated model-dependent uncertainty based on our acceptance and the decay topology, or, for those two-body modes where the angular distribution has been measured, the uncertainty due to the measured angular distribution.

V. THE DECAYS $\psi \to B_8\bar{B}_8$

In this section, we discuss decays of the type $\psi \to B_8\bar{B}_8$. We first discuss the decay

$$\psi \to p\bar{p} \,. \tag{5}$$

The invariant-mass distribution for all events with both a proton and antiproton identified by TOF is shown in Fig. 3(a), while Fig. 3(b) shows the mass distribution for two-prong $p\bar{p}$ events. There is a clear signal of events centered near 3.1 GeV/c^2, which we attribute to the decay (5).

For events with $3.02 < m(p\bar{p}) < 3.17$ GeV/c^2, we plot

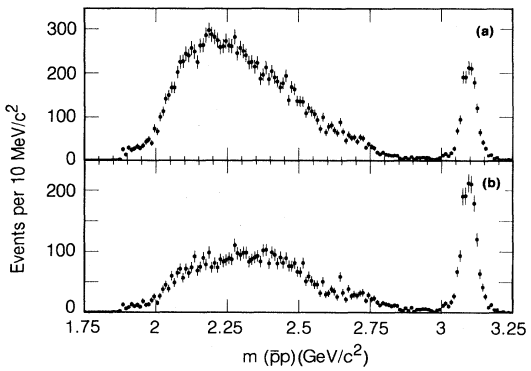

FIG. 3. (a) $p\bar{p}$ mass for all pairs and (b) two-prong events only. The peak near 3.1 GeV/c^2 is from the decay $\psi \to p\bar{p}$.

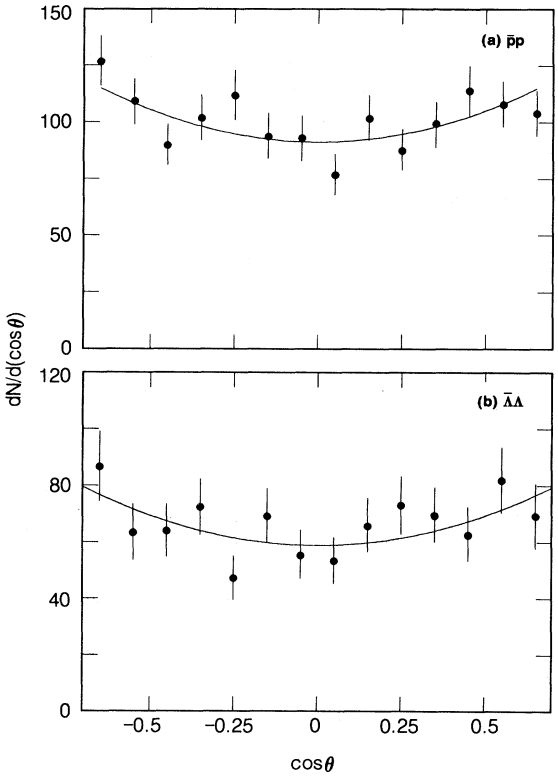

FIG. 4. (a) Angular distribution of $p\bar{p}$ pairs from the ψ and (b) angular distribution for $\psi \to \Lambda\bar{\Lambda}$ (arbitrary units). Solid curves are fits described in the text.

$dN/d(\cos\theta)$ of the pair in Fig. 4(a), where θ is the angle between the proton direction and the positron beam direction. Since the acceptance is constant in the region $|\cos\theta| < 0.7$, we may determine the angular distribution of $p\bar{p}$ pairs directly from the detected distribution. A fit of the form

$$\frac{dN}{d(\cos\theta)} = N_0(1+\alpha\cos^2\theta) \tag{6}$$

gives

$$\alpha = 0.61 \pm 0.23 \,. \tag{7}$$

The branching ratio is

$$B(\psi \to p\bar{p}) = (2.16 \pm 0.07 \pm 0.15)\times10^{-3} \,, \tag{8}$$

where in this and all following cases the first error is statistical and the second is systematic. Note again that the systematic error includes errors in normalization, angular distribution, and the Monte Carlo simulation.

Figure 5 shows the inclusive momentum spectrum of Λ and $\bar{\Lambda}$ at the ψ, where we have imposed the additional requirement that the decay vertex lie at least 8 mm in the radial direction from the IP. There is a clear enhancement centered near $p = 1.07$ GeV/c, which corresponds to the decay

$$\psi \to \Lambda\bar{\Lambda} \,. \tag{9}$$

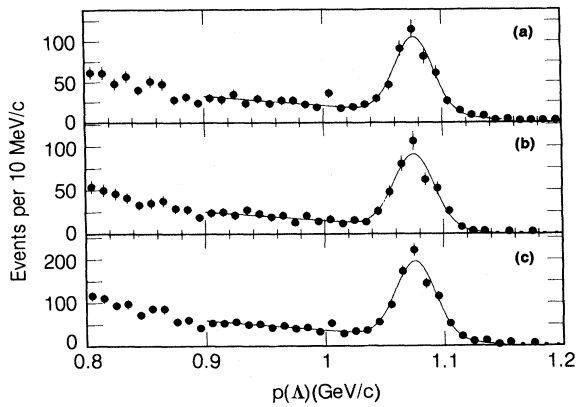

FIG. 5. Inclusive momentum spectrum of Λ or $\bar{\Lambda}$ at the ψ, (a) Λ, (b) $\bar{\Lambda}$, and (c) both Λ and $\bar{\Lambda}$ added. The peak near 1.08 GeV/c is due to the decay $\psi\to\Lambda\bar{\Lambda}$. Solid curve is fit described in text.

For events which have a Λ or $\bar{\Lambda}$ with $1.05<p<1.12$ GeV/c, we form the angular distribution of the Λ direction, shown in Fig. 4(b). Only one Λ per event is allowed to enter the plot if both are reconstructed. The acceptance-corrected distribution is fit to the hypothesis (6), which yields the result

$$\alpha=0.72\pm0.36\ . \tag{10}$$

We individually fit the momentum distribution for each charge mode, correct for acceptance, and combine the results to obtain

$$B(\psi\to\Lambda\bar{\Lambda})=(1.58\pm0.08\pm0.19)\times10^{-3}\ . \tag{11}$$

We now turn our attention to the decay

$$\psi\to\Sigma^0\bar{\Sigma}^0\ . \tag{12}$$

Figure 6 shows the $\Lambda\bar{\Lambda}$ invariant-mass distribution for all events with both a reconstructed Λ and a $\bar{\Lambda}$, where the Λ and $\bar{\Lambda}$ are selected only by invariant-mass cuts. There is clear evidence for a peak centered near 3.1 GeV/c^2 from the decay $\psi\to\Lambda\bar{\Lambda}$, a broader peak centered near 2.9 GeV/c^2, and a very broad line shape lying below 2.8 GeV/c^2, to be discussed later.

We now discuss the enhancement between 2.8 and 3 GeV/c^2. Due to the small Q involved in Σ^0 decay, essentially all events from reaction (12) have $2.8<m(\Lambda\bar{\Lambda})<3.0$ GeV/c^2. There are two other possible sources for events in this region. The decays

$$\psi\to\Lambda\bar{\Lambda}\pi^0 \tag{13}$$

and

$$\psi\to\Lambda\bar{\Sigma}^0 \tag{14}$$

are isospin forbidden and as such are strongly suppressed.[26] As a result, the events in the region $2.84<m(\Lambda\bar{\Lambda})<2.96$ GeV/c^2 are predominantly from the decay (12).

Since the Σ^0 is never actually reconstructed, we use the Λ from the Σ^0 decay to measure the Σ^0 direction. Due to the small Q of the Σ^0 decay, the laboratory angle between the Λ and the Σ^0 is always less than 4°. Thus, to a very good approximation, the Λ direction mimics the Σ^0 direction. Figure 7(a) shows the folded $\Sigma^0\bar{\Sigma}^0$ angular distribution, corrected for acceptance. A fit of the form

$$\frac{dN}{d\,|\cos\theta|}=N_0(1+\alpha\cos^2\theta) \tag{15}$$

is done to the angular distribution, from which we get

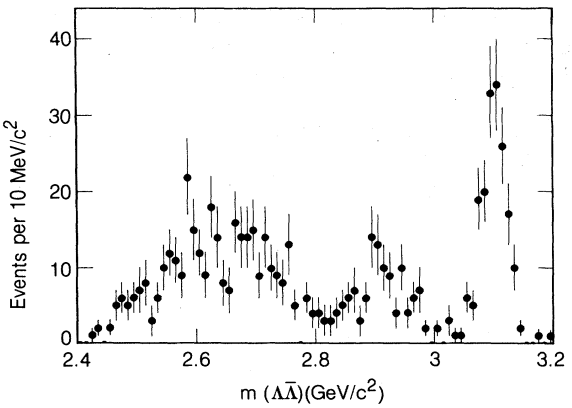

FIG. 6. $m(\Lambda\bar{\Lambda})$ for all events. The peak near 3.1 GeV/c^2 is from the decay $\psi\to\Lambda\bar{\Lambda}$, the peak near 2.9 GeV/$c^2$ is from the decay $\psi\to\Sigma^0\bar{\Sigma}^0$, and the enhancement below 2.8 GeV/c^2 is discussed in the text.

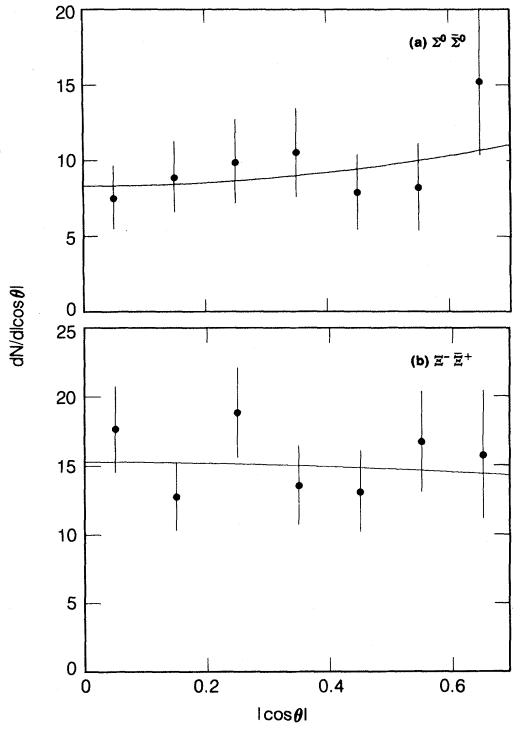

FIG. 7. (a) $\psi\to\Sigma^0\bar{\Sigma}^0$ angular distribution and (b) angular distribution for $\psi\to\Xi^-\bar{\Xi}^+$ (arbitrary units). Solid curves are fits described in text. The angular distributions have been reflected about zero due to low statistics.

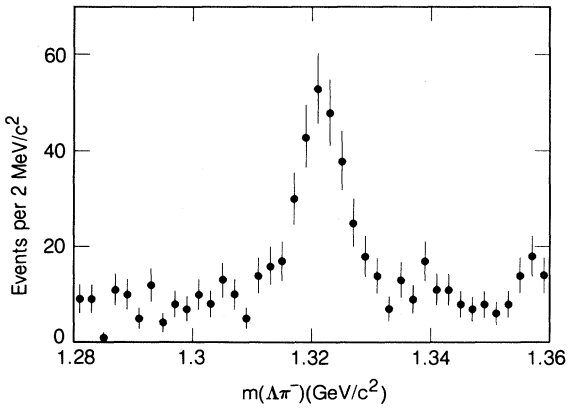

FIG. 8. $m(\Lambda\pi^-)$. The peak near 1.321 GeV/c^2 is from the decay $\Xi^-\to\Lambda\pi^-$. Here and in all subsequent figures, the charge-conjugate mode is implied, unless stated to the contrary.

$$\alpha=0.7\pm1.1\ . \tag{16}$$

This yields the result

$$B(\psi\to\Sigma^0\bar{\Sigma}^0)=(1.58\pm0.16\pm0.25)\times10^{-3}\ . \tag{17}$$

Finally, we discuss the decay

$$\psi\to\Xi^-\bar{\Xi}^+\ . \tag{18}$$

Here, and in what follows, we designate the antibaryon charge with the actual charge of the antiparticle, i.e., the $\bar{\Xi}^+$ is the antiparticle of the Ξ^-. Figure 8 shows the invariant mass for $\Lambda\pi^-$ events, where no distance of closest approach cuts are made on the additional π^- from the weak decay of the Ξ^-. There is a clear enhancement, centered near 1.32 GeV/c^2, indicating Ξ^- production. For events with $1.312<m(\Lambda\pi^-)<1.33$ GeV/c^2, the three-body mass is set to the Ξ^- mass, and the Ξ^- energy is recalculated. Figure 9 shows the missing mass m_m opposite the Ξ^- system. There is a clear enhancement, centered near 1.32 GeV/c^2, which comes from the decay (18). Figure 10 shows a beautiful example of a $\psi\to\Xi^-\bar{\Xi}^+$ event.

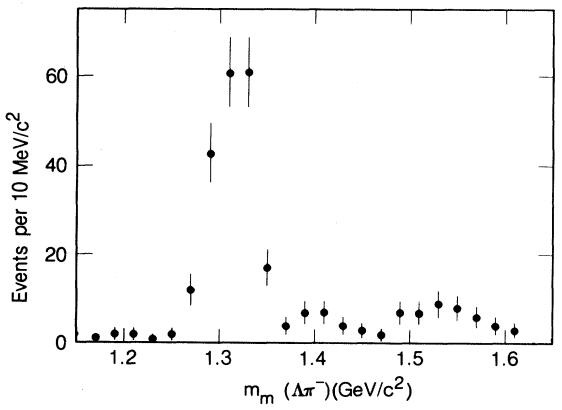

FIG. 9. Missing mass against Ξ^-. The peak near 1.32 GeV/c^2 is from the decay $\psi\to\Xi^-\bar{\Xi}^+$, while the enhancement above 1.48 GeV/c^2 is discussed in the text.

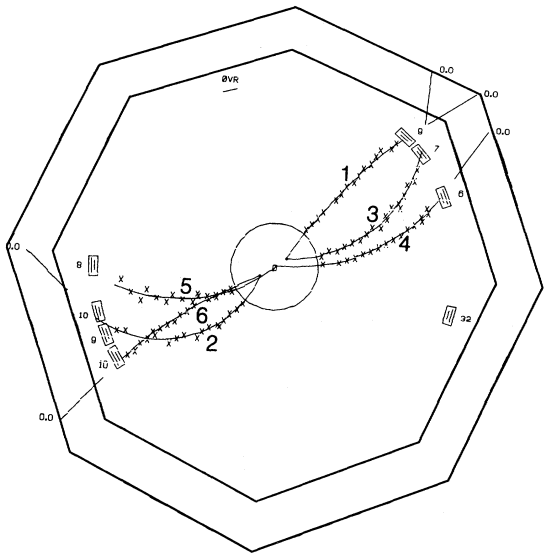

FIG. 10. An example of a fully reconstructed $\psi\to\Xi^-\bar{\Xi}^+$ event. Both Λ's decay over 10 cm from the primary vertex, and the Ξ vertices are visible as neither of the other two pions seem to come from the primary vertex. Track 1 is an antiproton, track 6 is a proton, tracks 3 and 4 are π^+'s, and tracks 2 and 5 are π^-'s. A dot has been sketched to indicate the Λ vertices. The numbers next to the small rectangular boxes give the approximate TOF in ns. The liquid-argon modules were inoperative during this run and hence do not register energy deposition, indicated by the 0.0 next to each of the charged tracks in the LA system.

The events of Fig. 9 in the vicinity of $m_m(\Xi^-)=1.38$ GeV/c^2 are from background under the Ξ^- peak. The events with $m_m(\Xi^-)>1.5$ GeV/c^2 are due to the decay

$$\psi\to\Xi^-\bar{\Xi}^+\pi^0\ , \tag{19}$$

or possibly the SU(3)$_f$-forbidden decay

$$\psi\to\Xi^-\bar{\Xi}^+(1530)\ . \tag{20}$$

Reaction (20) is of particular interest due to the results in Sec. VII on SU(3)$_f$-forbidden decays, but it is difficult to make a positive identification due to its low efficiency and the background from reaction (19). This experiment cannot separate the two contributions.

For events which have $1.26<m_m(\Xi^-)<1.36$ GeV/c^2, we plot in Fig. 7(b) the folded angular distribution, corrected for acceptance. A fit done to the hypothesis (15), gives the result

$$\alpha=-0.13\pm0.55\ , \tag{21}$$

and the branching ratio is

$$B(\psi\to\Xi^-\bar{\Xi}^+)=(1.14\pm0.08\pm0.20)\times10^{-3}\ . \tag{22}$$

Returning to Fig. 6, we discuss the region below 2.8 GeV/c^2. Any decay which has a final-state topology of $\Lambda\bar{\Lambda}\pi\pi$ will populate the region below 2.8 GeV/c^2. If the decay

TABLE II. Reduced branching fractions $|M|^2$ for $\psi \to B_8\bar{B}_8$ (units of 10^{-3}).

Decay mode	Value
$\psi \to p\bar{p}$	1.73±0.13
$\psi \to \Lambda\bar{\Lambda}$	1.45±0.18
$\psi \to \Sigma^0\bar{\Sigma}^0$	1.58±0.30
$\psi \to \Xi^-\bar{\Xi}^+$	1.39±0.26

$$\psi \to \Xi^0\bar{\Xi}^0 \tag{23}$$

occurs with the same strength as the decay $\psi \to \Xi^-\bar{\Xi}^+$ (18), as one would expect from isospin considerations, then we would expect a total of 126±14 events with $m(\Lambda\bar{\Lambda}) < 2.8$ GeV/c^2 from decays (18) and (23), where in fact there are 326±18 events. It is clear that there are substantial contributions below 2.8 GeV/c^2 from other processes than decays (18) and (23), including decays discussed in Sec. VI, such as (28) and (30).

We now compare the results of this section. Table II shows the reduced branching fraction $|M|^2$ for all decays of the type

$$\psi \to B_8\bar{B}_8 \tag{24}$$

where we have divided[27] out the phase-space factor of

$$R_2 = \frac{\pi p}{\sqrt{s}} , \tag{25}$$

corresponding to two-body phase space, and have combined in quadrature statistical and systematic errors. Here p is the momentum of the final-state particle in the ψ rest system. As mentioned in the Introduction, if the ψ is an $SU(3)_f$ singlet, the matrix elements for $\psi \to B_8\bar{B}_8$ should be the same. All four of the reduced branching fractions in Table II are consistent with the ψ being a pure $SU(3)_f$ singlet.

Table III summarizes the measurements of angular distributions for the decays $\psi \to B_8\bar{B}_8$. These are compared to two recent calculations, one[28] in the asymptotic limit, and the other[29] including mass effects. The data tend to prefer the latter calculation.

VI. THE DECAYS $\psi \to B_{10}\bar{B}_{10}$

We now turn our attention to decays of the type $\psi \to B_{10}\bar{B}_{10}$. The decay

$$\psi \to \Delta^{++}\bar{\Delta}^{--} \tag{26}$$

TABLE III. Angular distributions for $\psi \to B_8\bar{B}_8$ (α for $1+\alpha\cos^2\theta$ angular distribution).

Decay mode	This experiment	Ref. 28	Ref. 29
$\psi \to p\bar{p}$	0.61±0.23	1	0.46
$\psi \to \Lambda\bar{\Lambda}$	0.72±0.36	1	0.32
$\psi \to \Sigma^0\bar{\Sigma}^0$	0.7±1.1	1	0.31
$\psi \to \Xi^-\bar{\Xi}^+$	−0.13±0.59	1	0.16

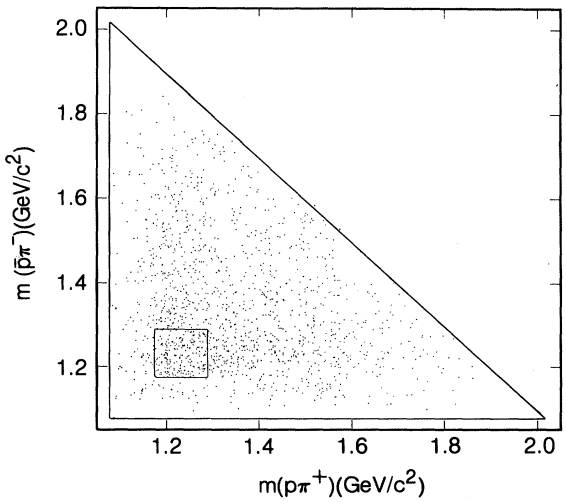

FIG. 11. Goldhaber plot of $m(p\pi^+)$ vs $m(\bar{p}\pi^-)$ from the decay $\psi \to p\bar{p}\pi^+\pi^-$. Box is $\psi \to \Delta^{++}\bar{\Delta}^{--}$ signal region.

naturally arises out of analysis of the reaction $\psi \to p\bar{p}\pi^+\pi^-$ (73), discussed in Sec. X. Figure 11 shows the Goldhaber plot for doubly charged $p\pi$ combinations for reaction (73), while Fig. 12 shows the summed $p\pi^+$ projections of Fig. 11, illustrating a strong Δ^{++} signal. We define the square bounded by $1.18 < m(p\pi^+) < 1.32$ GeV/c^2 in Fig. 11 as the signal region for reaction (26). The Monte Carlo simulation is used as an estimate of the nonresonant background population. This takes into account not only the nonuniform phase space inherent in the Goldhaber plot, but also acceptance variations over the plot. The background subtraction yields the result

$$B(\psi \to \Delta^{++}\bar{\Delta}^{--}) = (1.10 \pm 0.09 \pm 0.28) \times 10^{-3} . \tag{27}$$

The decay mode

$$\psi \to \Sigma^-(1385)\bar{\Sigma}^+(1385) \tag{28}$$

is observed. The inclusive $\Lambda\pi^-$ mass spectrum has been replotted in Fig. 13(a). There is a narrow Ξ^- peak, dis-

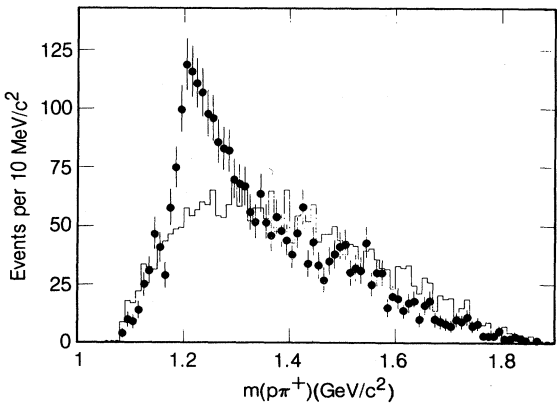

FIG. 12. $m(p\pi^+)$ for $\psi \to p\bar{p}\pi^+\pi^-$ events. The peak near 1.23 GeV/c^2 is from the decay $\Delta^{++} \to p\pi^+$. Solid histogram is phase-space distribution normalized to same number of events.

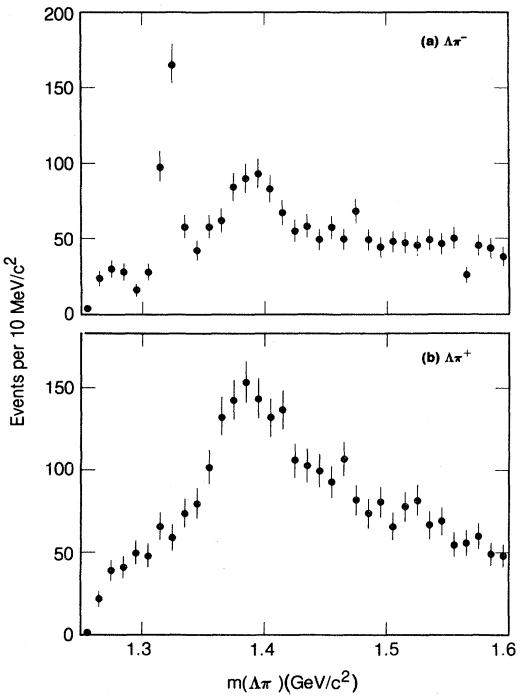

FIG. 13. (a) $m(\Lambda\pi^-)$ and (b) $m(\Lambda\pi^+)$. The peak near 1.32 GeV/c^2 in (a) is from the decay $\Xi^-\to\Lambda\pi^-$, while the peak near 1.38 GeV/c^2 in both (a) and (b) is from the decay $\Xi(1385)\to\Lambda\pi$.

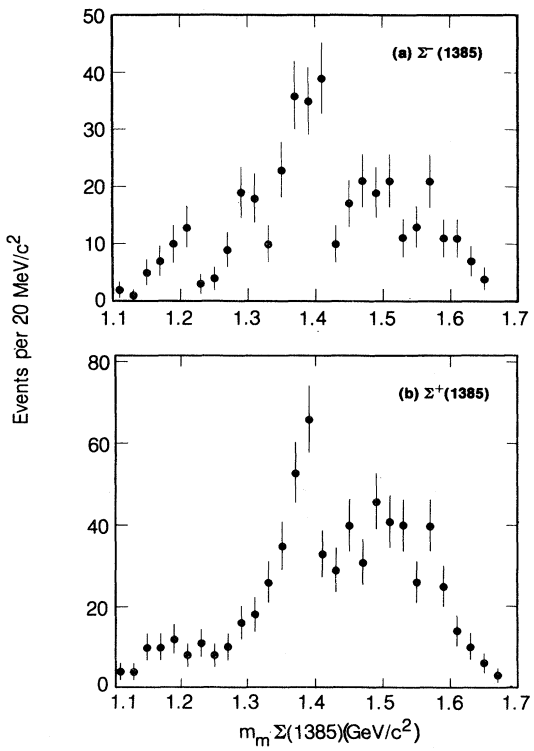

FIG. 14. (a) Missing mass against $\Sigma^-(1385)$ and (b) missing mass against $\Sigma^+(1385)$. The peaks near 1.38 GeV/c^2 in both (a) and (b) are due to the decays $\psi\to\Sigma(1385)\bar{\Sigma}(1385)$, while the peaks near 1.19 GeV/c^2 in both (a) and (b) are primarily due to reactions (33) and (35). Here, we denote as $\Sigma(1385)$ a $\Lambda\pi$ system in the mass region defined in the text.

cussed in Sec. V, and a broader peak centered near 1.38 GeV/c^2, which we attribute to the P'_{13} $I=1$ strange baryon resonance, the $\Sigma^-(1385)$. For events with $1.36<m(\Lambda\pi^-)<1.41$ GeV/c^2, we plot the missing mass against the $\Sigma^-(1385)$, shown in Fig. 14(a). There is clear evidence of a peak near 1.38 GeV/c^2, which comes from reaction (28). The background subtraction assumes a smooth curve above and below the $\Sigma^-(1385)$ and yields the result

$$B(\psi\to\Sigma^-(1385)\bar{\Sigma}^+(1385))=(0.86\pm0.18\pm0.22)\times10^{-3}\ . \tag{29}$$

We can also perform the analogous analysis for the charge-symmetric mode of reaction (28). The invariant mass of the $\Lambda\pi^+$ system is shown in Fig. 13(b). There is a clear peak centered near 1.38 GeV/c^2, indicating $\Sigma^+(1385)$ production on top of a substantial combinatoric background. This distribution differs from that in Fig. 13(a) in that there is no corresponding state to the Ξ^-. The missing mass for events with $1.36<m(\Lambda\pi^+)<1.41$ GeV/c^2, is shown in Fig. 14(b). There is a peak centered near 1.38 GeV/c^2, indicating the decay

$$\psi\to\Sigma^+(1385)\bar{\Sigma}^-(1385)\ . \tag{30}$$

A similar background subtraction as above yields the result

$$B(\psi\to\Sigma^+(1385)\bar{\Sigma}^-(1385))=(1.03\pm0.24\pm0.25)\times10^{-3}\ . \tag{31}$$

We now make the same comparison for the decays

$$\psi\to B_{10}\bar{B}_{10}\ , \tag{32}$$

as was done for the octet baryons in Sec. V. Table IV shows the reduced matrix elements for decays of the type (32). The three measurements in Table IV are also in good agreement with each other, again consistent with the ψ being a pure $SU(3)_f$ singlet. In particular, there is no evidence for isospin violation in the comparison of reactions (28) and (30).

VII. THE DECAYS $\psi\to B_8\bar{B}_{10}$

We now investigate the $SU(3)_f$-forbidden decays of the type $\psi\to B_8\bar{B}_{10}$. As mentioned in the Introduction, such decays should be strongly suppressed, and the observation of such decays is the first indication of a substantial branching fraction for a $SU(3)_f$-forbidden decay.

TABLE IV. Reduced branching fractions $|M|^2$ for $\psi\to B_{10}\bar{B}_{10}$ for (units of 10^{-3}).

Decay mode	Value
$\psi\to\Delta^{++}\bar{\Delta}^{--}$	1.12±0.30
$\psi\to\Sigma^-(1385)\bar{\Sigma}^+(1385)$	1.21±0.40
$\psi\to\Sigma^+(1385)\bar{\Sigma}^-(1385)$	1.48±0.46

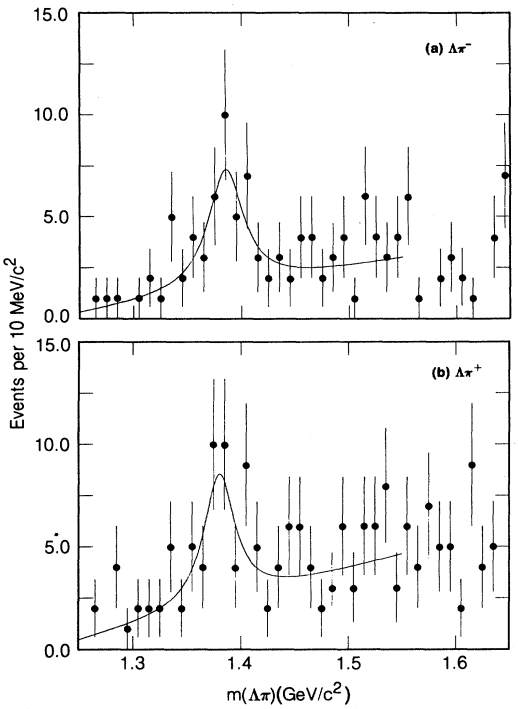

FIG. 15. (a) $\Lambda\pi^-$ mass opposite Σ recoil and (b) $\Lambda\pi^+$ mass opposite Σ recoil. The peaks near 1.38 GeV/c^2 in (a) and (b) are from the decays $\psi\to\Sigma\bar{\Sigma}(1385)$. Solid lines are fits described in the text.

The first decay mode to be discussed is

$$\psi\to\Sigma^-(1385)\bar{\Sigma}^+ . \tag{33}$$

The $\Sigma^-(1385)$ is detected by its $\Lambda\pi^-$ decay mode. Events are selected as for the reaction

$$\psi\to\Lambda\bar{\Sigma}^+\pi^- , \tag{55}$$

discussed in Sec. IX below. We choose $\Lambda\pi^-$ events which have $1.14<m_m(\Lambda\pi^-)<1.24$ as having a $\bar{\Sigma}^+$ recoiling against them. Figure 15(a) shows the $\Lambda\pi^-$ mass opposite the $\bar{\Sigma}^+$ recoil. If indeed these events have a $\bar{\Sigma}^+$ recoiling against the $\Lambda\pi^-$ system, the events should all have at most four charged tracks in them, as the charged $\bar{\Sigma}^+$ always decays to $\bar{N}\pi$. In addition, some fraction of the time a charged track from the $\bar{\Sigma}^+$ decay should miss the IP as the $\bar{\Sigma}^+$ decays weakly. The events have been hand scanned and are topologically consistent with the event hypothesis. Thus, Fig. 15(a) provides good evidence for the SU(3)$_f$-forbidden reaction (33). We fit the peak, using a Breit-Wigner form of width $\Gamma=40$ MeV/c^2, which gives the result

$$B(\psi\to\Sigma^-(1385)\bar{\Sigma}^+)=(0.29\pm0.11\pm0.10)\times10^{-3} . \tag{34}$$

We now search for the analogous SU(3)$_f$-forbidden effect in the charge-symmetric mode

$$\psi\to\Sigma^+(1385)\bar{\Sigma}^- . \tag{35}$$

Again, events are selected as in Sec. IX below for the decay

TABLE V. Reduced branching fractions $|M|^2$ for $\psi\to B_8\bar{B}_{10}$ (units of 10^{-3}).

Decay mode	Value
$\psi\to\Sigma^-(1385)\bar{\Sigma}^+$	0.37±0.20
$\psi\to\Sigma^+(1385)\bar{\Sigma}^-$	0.39±0.20

$$\psi\to\Lambda\bar{\Sigma}^-\pi^+ . \tag{57}$$

We choose events which have $1.14<m_m(\Lambda\pi^+)<1.24$ as having a $\bar{\Sigma}^-$ recoiling against them. Figure 15(b) shows the $\Lambda\pi^+$ mass opposite the $\bar{\Sigma}^-$ recoil. There is again good evidence for the SU(3)$_f$-forbidden reaction (35). We fit the peak in the same way as for the charge-symmetric mode, which gives the result

$$B(\psi\to\Sigma^+(1385)\bar{\Sigma}^-)=(0.31\pm0.11\pm0.11)\times10^{-3} . \tag{36}$$

The fact that we see the same SU(3)$_f$-forbidden effect in two independent modes at the same strength is strong corroboration of this striking result.

As was done in Secs. V and VI, we compare the reduced matrix elements for

$$\psi\to B_8\bar{B}_{10} , \tag{37}$$

shown in Table V. The magnitude of the SU(3)$_f$-forbidden effect is large especially when compared with the results in Tables II and IV. This indicates a sizable SU(3)$_f$ violation in the two-body decays of the ψ. It is interesting that SU(3)$_f$-forbidden effects do not seem to be present in those channels where there is an SU(3)$_f$-allowed amplitude. Note that while we cannot prove the existence of the reaction $\psi\to\Xi^-\bar{\Xi}^+(1530)$ (18), which is another SU(3)$_f$-forbidden reaction, the data cannot rule out the presence of this reaction at a level comparable to that of reactions (34) and (36).

VIII. RADIATIVE DECAYS OF THE ψ

In this section, we search for exclusive radiation decays of the ψ, predicted to first order in QCD. The search encompasses charged-particle states opposite the direct photon. Events from the decay

$$\psi\to p\bar{p}\gamma \tag{38}$$

are detected by observing a single photon opposite the $p\bar{p}$ state. More than one photon per event is allowed due to noise in the LA shower counters. Events from the decay $\psi\to p\bar{p}$ are eliminated by requiring $m(p\bar{p})<2.97$ GeV/c^2. We cut on the kinematics of the two-prong $p\bar{p}$ system to eliminate multipion final states. The variable $U\equiv E_m-p_mc$ is used, where E_m and p_m are, respectively, the missing energy and missing momentum opposite the $p\bar{p}$ system. We accept a region of $-0.07<U<0.06$ GeV, which corresponds to a longitudinal band near the bottom of Fig. 16. Note that U is related to $m_m{}^2$ by the relationship

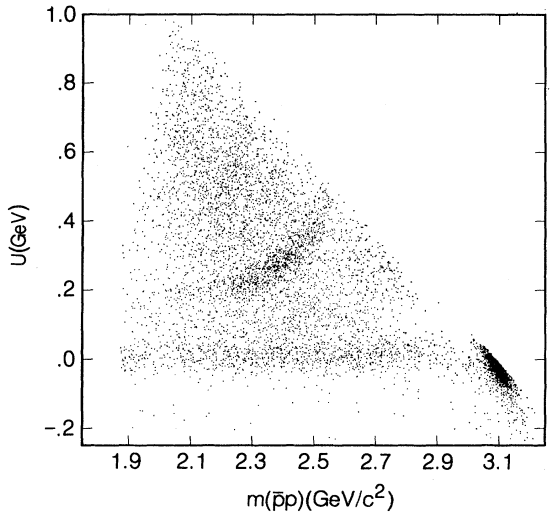

FIG. 16. Scatterplot of $p\bar{p}$ mass versus U, in all $p\bar{p}$ pairs. The band in the vicinity of $U=0.3$ GeV is due to the decay $\psi\to p\bar{p}\eta$, while the band near $U=0$ GeV is due to the decays $\psi\to p\bar{p}\gamma(\pi^0)$. The dark region near $m(p\bar{p})=3.1$ GeV/c^2 is from the decay $\psi\to p\bar{p}$.

$$m_m{}^2c^4=E_m{}^2-p_m{}^2c^2$$
$$=(E_m+p_mc)U\ . \tag{39}$$

The advantage of the variable U is that the error in the quantity U is to first order independent of the energy of the missing $\gamma(\pi^0)$, whereas the error in $m_m{}^2$ increases with the energy of the missing $\gamma(\pi^0)$. The U cut essentially removes all multipion final states opposite the proton-antiproton pair, while losing very little of the single $\gamma(\pi^0)$ signal.

It is impossible to discriminate between reaction (38) and the reaction

$$\psi\to p\bar{p}\pi^0 \tag{40}$$

in the Mark II detector without photon detection, as the resolution in $m_m{}^2$ is not sufficient. Events from (40) are suppressed by using the transverse momentum squared q^2 of the photon relative to the missing momentum, defined as

$$q^2=4p_m{}^2\sin^2\frac{\chi}{2}\ , \tag{41}$$

where χ is the angle between the observed photon direction and the direction of the missing momentum of the $p\bar{p}$ system. The q^2 distribution of the observed photon is shown in Fig. 17. The q^2 distributions for reactions (38) and (40) exhibit markedly different characteristics.[30] The q^2 distribution of direct-photon events is very strongly peaked, with $\simeq$80% of the events having $q^2<0.001$ (GeV/c)^2, while the q^2 distribution of π^0 events is much broader. The large excess of events with $q^2<0.001$ (GeV/c)^2 in Fig. 17 arises from the decay (38). This region will subsequently be referred to as the direct-photon-signal region.

We have determined[25] the contribution to the signal region from false photons due to noise in the LA system to be small. The feedthrough from reaction (40) is estimated from the population in the region $0.003<q^2<0.01$ (GeV/c)^2, where the direct-photon contribution is negligible. The corresponding contribution for $q^2<0.001$ (GeV/c)^2 is removed. The resulting branching fraction is

$$B(\psi\to p\bar{p}\gamma)=(0.38\pm0.07\pm0.07)\times10^{-3}\ . \tag{42}$$

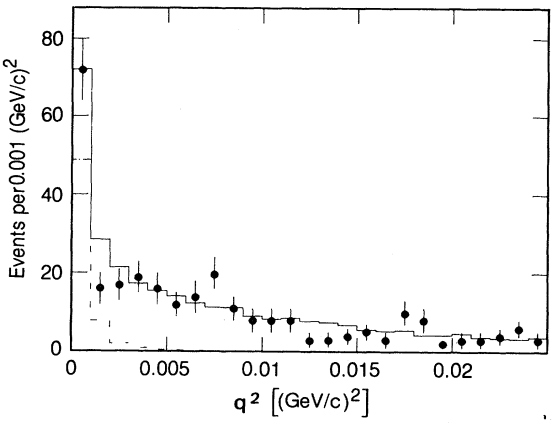

FIG. 17. q^2 distribution of observed photons from $\psi\to p\bar{p}\gamma(\pi^0)$ events. Solid histogram is expected contribution from sum of π^0 and γ decays, discussed in text. Dashed histogram is direct-photon contribution only.

If the direct-photon decay proceeds via $\psi\to gg\gamma$, where the final-state hadrons result from the fragmentation of the two gluons in a color singlet state, the possibility of a two-gluon bound state exists.[2,14] The unsubtracted $p\bar{p}$ mass spectrum is shown in Fig. 18. The spectrum shows no obvious structure, although it is consistent with an enhancement just above threshold, as discussed below in Sec. IX.

We may also determine the branching fraction for $\psi\to p\bar{p}\pi^0$ (40) using the q^2 distribution. The region beyond $q^2=0.003$ (GeV/c)^2 is essentially free of other

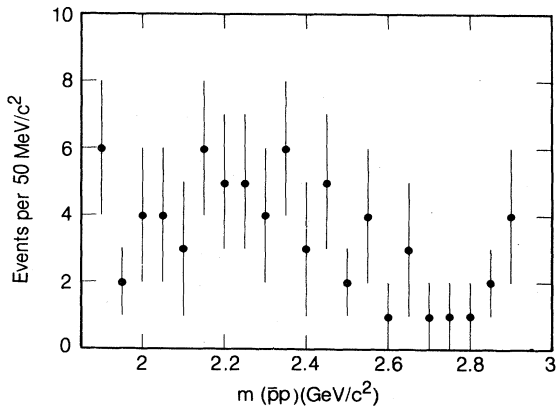

FIG. 18. Mass of $p\bar{p}$ pairs opposite direct photons. The rise near 2.9 GeV/c^2 is probably due to $\psi\to p\bar{p}$ events coupling with noise photons, as the q^2 cut is not very stringent for low-momentum photons.

backgrounds, and yields a result consistent with the result obtained in Sec. IX without use of the LA system. This result is a good confirmation of the performance of the LA shower counters as estimated by the simulation.

The Mark I experiment reported[31]

$$B(\psi\to p\bar{p}\gamma)<0.11\times10^{-3} \tag{43}$$

($\pm15\%$ systematic errors) as the 90%-C.L. upper limit. The γ branching fraction (42) is a factor of 3 larger than the Mark I upper limit (43). The Mark II shower-counter efficiency has been found to be in good agreement with the Monte Carlo simulation, and consequently we are confident of the result (42).

We have also looked for direct-photon decays of the ψ in the four-prong exclusive channel with two charged pions in addition to the dibaryon system. The selection criteria for this channel are completely analogous to that for the decay $\psi\to p\bar{p}\gamma$ (38). For these events, we plot the quantity U for the $p\bar{p}\pi^+\pi^-$ system, shown in Fig. 19. Events from the decay $\psi\to p\bar{p}$ are eliminated by requiring $m(p\bar{p})<2.99$ GeV/c^2. There is a clear band of events located near the bottom of Fig. 19, which is consistent with the decays

$$\psi\to p\bar{p}\pi^+\pi^-\gamma \tag{44}$$

and

$$\psi\to p\bar{p}\pi^+\pi^-\pi^0\ . \tag{45}$$

Figure 20 shows the q^2 of the observed photon relative to the missing momentum of the $p\bar{p}\pi^+\pi^-$ system. Events with four-prong mass >2.99 GeV/c^2 have been eliminated to remove $\psi\to p\bar{p}\pi^+\pi^-$ events. There is no evidence[32] for a direct photon opposite the $pp^-\pi^+\pi^-$ system.

Taking $q^2<1\times10^{-3}$ (GeV/c)^2 as the signal region, we place a limit of

$$B(\psi\to p\bar{p}\pi^+\pi^-\gamma)<0.79\times10^{-3} \tag{46}$$

at the 90% confidence level.

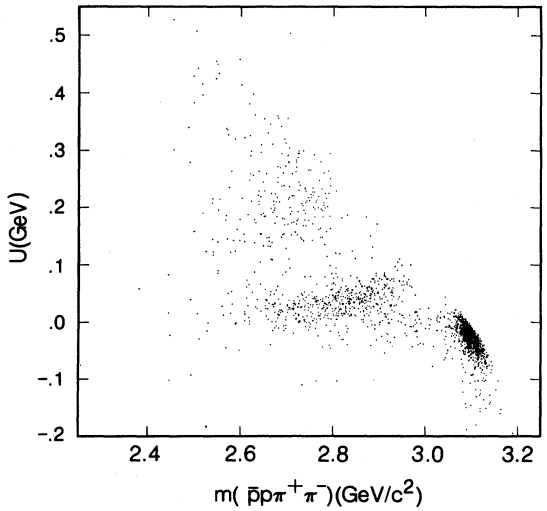

FIG. 19. Scatter plot of the quantity U vs $m(p\bar{p}\pi^+\pi^-)$. The band near $U=0$ is from the decays $\psi\to p\bar{p}\pi^+\pi^-\gamma(\pi^0)$, while the dot near 3.1 GeV/c^2 is from the decay $\psi\to p\bar{p}\pi^+\pi^-$.

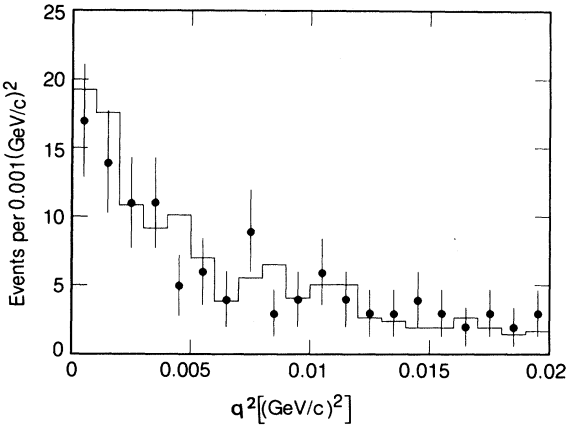

FIG. 20. q^2 of observed photon in $\psi\to p\bar{p}\pi^+\pi^-\gamma(\pi^0)$ events. Histogram is expected contribution from $\psi\to p\bar{p}\pi^+\pi^-\pi^0$.

IX. THREE-BODY DECAY MODES OF THE ψ

We now turn our attention to the large variety of three-body decay modes of the ψ. As will be shown, nearly all three-body decay modes with a baryon-antibaryon pair which are allowed proceed at a rate of order 1×10^{-3}. We first discuss the reaction

$$\psi\to p\bar{p}\pi^0\ . \tag{40}$$

As previously mentioned, we cannot separate the reaction $\psi\to p\bar{p}\gamma$ (38) from the decay $\psi\to p\bar{p}\pi^0$ (40) without photon detection. The contribution from reaction (38) was ascertained in Sec. VIII, and the remainder of events in the region $-0.07<U<0.06$ of Fig. 16 are due to the decay (40). Events from the decay $\psi\to p\bar{p}$ are removed by requiring $m(p\bar{p})<2.99$ GeV/c^2. We take the U projection of Fig. 16, shown in Fig. 21. The bins about $U=0$ are fit to a Gaussian, shown as a solid line in Fig. 21. The expected feeddown from $\psi\to p\bar{p}\gamma$ (38) events is subtracted, which yields the result

$$B(\psi\to p\bar{p}\pi^0)=(1.13\pm0.09\pm0.09)\times10^{-3}\ . \tag{47}$$

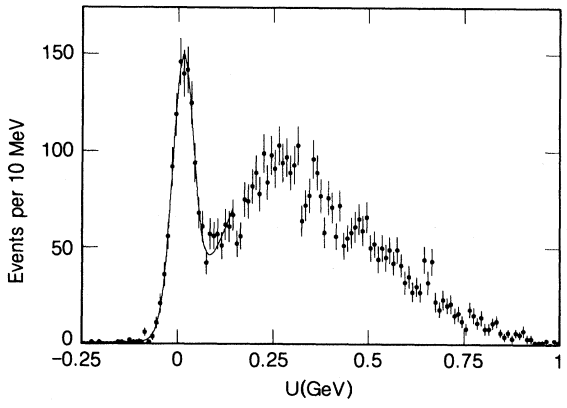

FIG. 21. The quantity U for all two-prong $p\bar{p}$ pairs with $m(p\bar{p})<2.97$ GeV/c^2. The peak near $U=0$ is from the decays $\psi\to p\bar{p}\gamma(\pi^0)$.

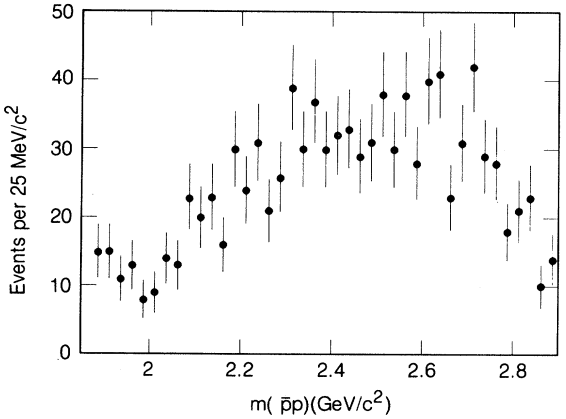

FIG. 22. $p\bar{p}$ mass for events consistent with a missing $\gamma(\pi^0)$. Note the enhancement near threshold.

Figure 22 shows the mass spectrum of $p\bar{p}$ pairs for those events consistent with either a missing π^0 or γ. A striking feature is a clear threshold enhancement for $p\bar{p}$ mass below 2 GeV/c^2. Note that the events in Fig. 22 are predominantly from $\psi\to p\bar{p}\pi^0$ (40), but that this threshold enhancement also shows up in Fig. 18, which is known to correspond to direct-photon events.

There is another argument which supports the interpretation of this enhancement as associated with a photon. If it were associated with a π^0, then the isoscalar nature of the γ demands the $p\bar{p}$ system be in an $I=1$ state. It must therefore also show up as an enhancement in the charge-symmetric reaction $\psi\to p\bar{n}\pi^-$ (48). The Dalitz plot in Fig. 24 shows no such enhancement at low $p\bar{n}$ mass as one would expect for an $I=1$ state.

We now turn our attention to the charge-symmetric three-body decay mode. The $m_m{}^2$ opposite the $p\pi^-$ system is shown in Fig. 23, for each charge mode separately as well as the sum. There exists a clear peak of events centered about $m_m{}^2=0.88$ (GeV/c^2)^2, which we attribute to the decay

$$\psi\to p\bar{n}\pi^- \ . \tag{48}$$

The $m_m{}^2$ spectrum of each charge mode is separately fit to account for differences due to nuclear interactions within the material between the interaction point and the first drift-chamber layer. Note that we do not assume the charge-conjugate mode in this paragraph. We obtain the results

$$B(\psi\to p\bar{n}\pi^-)=(2.02\pm0.07\pm0.16)\times10^{-3} \tag{49}$$

and

$$B(\psi\to\bar{p}n\pi^+)=(1.93\pm0.07\pm0.16)\times10^{-3} \ . \tag{50}$$

Since the ψ is an isoscalar, we can make an absolute prediction for the ratio of these two decays and the decay $\psi\to p\bar{p}\pi^0$ (40). From simple Clebsch-Gordan arguments, it follows that the branching fractions $\psi\to p\bar{p}\pi^0$, $\psi\to\bar{p}n\pi^+$, and $\psi\to p\bar{n}\pi^-$ should be in the ratios 1:2:2. The results of this experiment (47), (49), and (50) are 1:1.71±0.25:1.79±0.25, in good agreement with this prediction.

The events from reaction (48) are kinematically fit to the hypothesis $\psi\to p\bar{n}\pi^-$. For the 2356 events with suc-

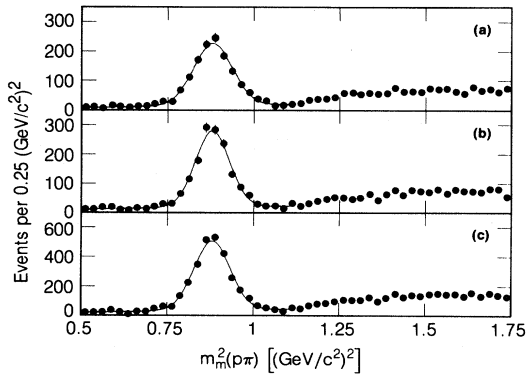

FIG. 23. $m_m{}^2$ against $N\pi$ system, (a) $p\pi^-$, (b) $\bar{p}\pi^+$, and (c) both charge modes. The peaks near $m_m{}^2=0.88$ (GeV/c^2)^2 are from the decays $\psi\to\bar{p}\pi^+n$. Solid curves are described in text.

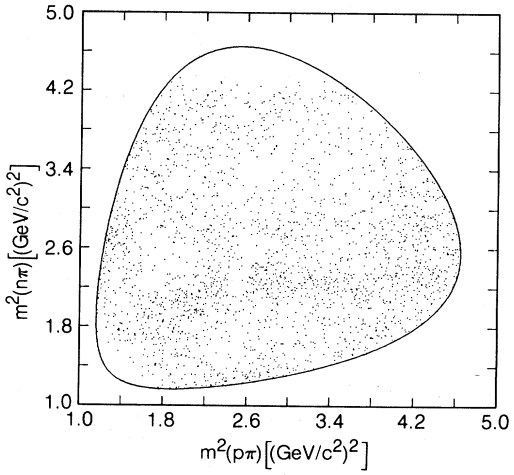

FIG. 24. Dalitz plot for $\psi\to\bar{p}n\pi^+$ and charge conjugate. The events in the plot are kinematically constrained to the event hypothesis.

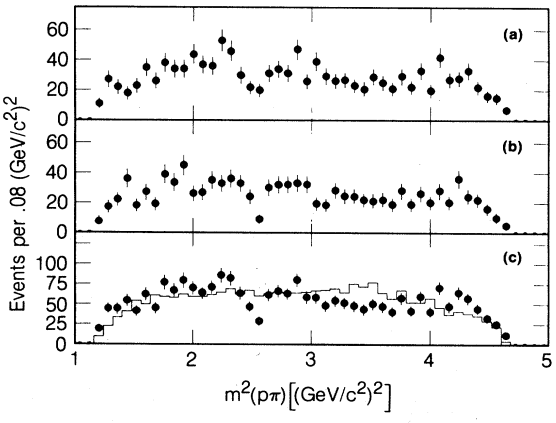

FIG. 25. Dalitz projections for $\psi\to\bar{p}n\pi^+$, (a) $p\pi^-$ projection, (b) $\bar{p}\pi^+$ projection, and (c) both charge modes added. The peak near $m_m{}^2=2.2$ (GeV/c^2)^2 are from the decays $\psi\to\bar{N}^0(1440-1535)n$. Solid histogram is phase-space prediction normalized to same number of events.

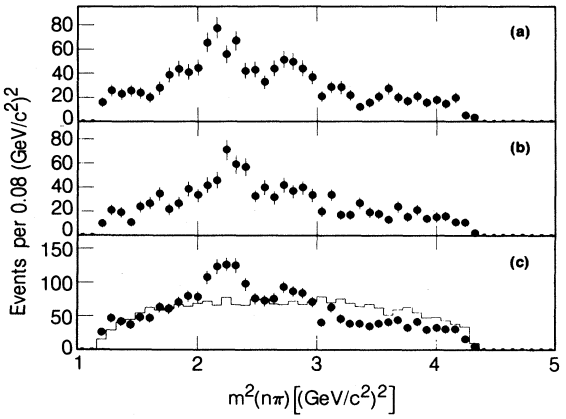

FIG. 26. Dalitz projections for $\psi\to\bar{p}n\pi^+$, (a) $\bar{n}\pi^-$ projection, (b) $n\pi^+$ projection, and (c) both modes added. The peaks near $m_m{}^2=2.2$ $(\mathrm{GeV}/c^2)^2$ are from the decays $\psi\to\bar{N}^-(1440-1535)p$. Other resonant structures may be present. Solid histogram is phase-space prediction normalized to same number of events.

cessful fits we form the Dalitz plot, shown in Fig. 24. The depopulations at high $m^2(\bar{n}\pi^-)$ and high $m^2(\bar{n}p)$ are due to the kinematic cutoffs for soft pions and protons in the apparatus. There is clear evidence for resonance formation in the $\bar{n}\pi^-$ system. The skew of the resonance band in the $\bar{n}\pi^-$ system near 2.2 $(\mathrm{GeV}/c^2)^2$ may be due to the interference of two similar ψ decay amplitudes with the same final state.

We note that if G parity is a good symmetry for the decay under study, then the Dalitz plot for Fig. 24 should be symmetric about the line $m^2(p\pi^-)=m^2(\bar{n}\pi^-)$, except for acceptance corrections. In addition, the Dalitz projections, shown in Figs. 25 and 26, should appear similar. There is clear evidence of a peak near 2.25 $(\mathrm{GeV}/c^2)^2$ in Fig. 26, which we attribute to the decay

$$\psi\to p\bar{N}^-(1440-1535)\,. \tag{51}$$

The evidence in Fig. 25 is less compelling. Here we denote[25] by $N(1440-1535)$ unresolved baryon resonances in the region of $m^2(n\pi^-)=2.25$ $(\mathrm{GeV}/c^2)^2$. In addition, there may[25] be other resonance behavior near 2.8 $(\mathrm{GeV}/c^2)^2$ in Fig. 26. In both cases there is evidence for destructive interference near 2.5 $(\mathrm{GeV}/c^2)^2$. The background is estimated by comparison with the phase-space Monte Carlo simulation, modified by the observed shape outside the resonance region. This yields

$$B(\psi\to p\bar{N}^-(1440-1535))=(0.93\pm0.15\pm0.32)\times10^{-3}\,. \tag{52}$$

Note that a number consistent with G-parity conservation is gotten from a similar analysis of the $p\pi^-$ channel.

A similar three-body decay mode of the ψ is the reaction

$$\psi\to\Delta^{++}\bar{p}\pi^-\,. \tag{53}$$

This decay mode arises naturally out of the discussion in Sec. X regarding the decay $\psi\to p\bar{p}\pi^+\pi^-$ (73). Figure 11 shows the distinct bands originating from Δ^{++} production. The reaction $\psi\to\Delta^{++}\bar{\Delta}^{--}$ (26) has been discussed in Sec. VI, and the remaining Δ^{++} production is due to reaction (53). The Monte Carlo simulation is used for an estimate of the nonresonant background, which yields the result

$$B(\psi\to\Delta^{++}\bar{p}\pi^-)=(1.58\pm0.23\pm0.40)\times10^{-3}\,. \tag{54}$$

We now investigate the decay

$$\psi\to\Lambda\bar{\Sigma}^+\pi^-\,. \tag{55}$$

Candidate events are selected by taking $\Lambda\pi^-$ events, where the π^- is required to satisfy the tight distance of closest approach cuts discussed in Sec. III. In addition, the π^- is required not to originate from another secondary vertex. Events with $1.3<m(\Lambda\pi^-)<1.32$ GeV/c^2 are removed to eliminate events originating from Ξ^- decays. For the remaining events, we plot the missing mass opposite the $\Lambda\pi^-$ system, shown in Fig. 27(a). There is a clear enhancement centered near 1.18 GeV/c^2, which comes from reaction (55), a smaller peak near 1.32 GeV/c^2 from feedthrough due to reaction $\psi\to\Xi^-\bar{\Xi}^+$

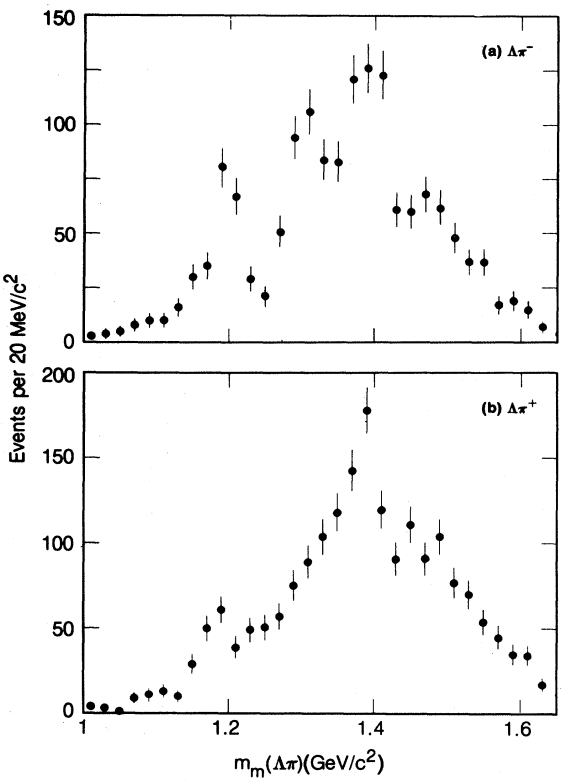

FIG. 27. (a) Missing mass opposite $\Lambda\pi^-$ events, where $\Xi^-\to\Lambda\pi^-$ events have been excluded and (b) missing mass opposite $\Lambda\pi^+$ events. The peak near 1.32 GeV/c^2 in (a) is from feedthrough of the decay $\psi\to\Xi^-\bar{\Xi}^+$, the peaks near 1.38 GeV/c^2 in (a) and (b) are due to the decays $\psi\to\Sigma(1385)\bar{\Sigma}(1385)$, and the peaks near 1.19 GeV/c^2 in (a) and (b) are due to the decays $\psi\to\Lambda\bar{\Sigma}\pi$.

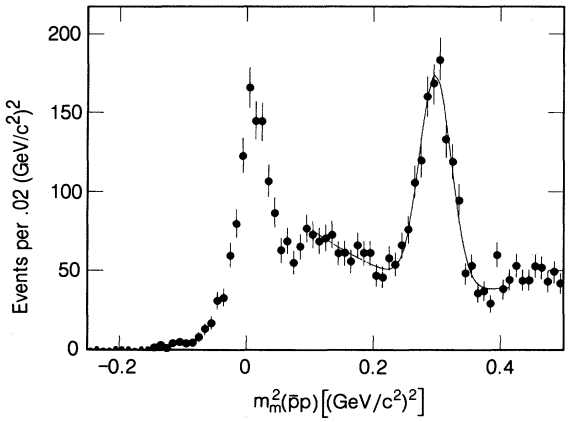

FIG. 28. $m_m{}^2$ against two-prong $p\bar{p}$ pairs at ψ. The peak near $m_m{}^2=0$ is from the decays $\psi\to p\bar{p}\gamma(\pi^0)$, while the peak near $m_m{}^2=0.3$ GeV/c^2 is from the decay $\psi\to p\bar{p}\eta$.

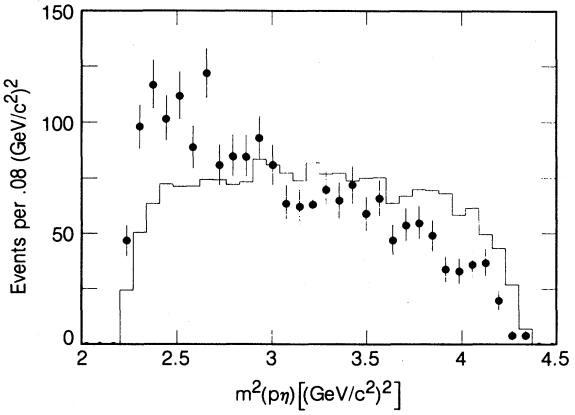

FIG. 30. $p\eta$ projection of $\psi\to p\bar{p}\eta$ Dalitz plot. The peak near the beginning of phase space is discussed in the text. Solid histogram is phase-space normalized to same number of events.

(18), as well as a peak near 1.38 GeV/c^2 from $\Xi^-(1385)$ production.

We now discuss the background subtraction. Events containing a real $\Lambda\pi^-$ must have either a $\bar{\Lambda}\pi^+$ or a stable particle like the $\bar{\Sigma}^+$ recoiling against it in order to simultaneously conserve charge, strangeness, and baryon number. As $\Lambda\pi^-$ threshold is about 1.25 GeV/c^2, the background must radically change slope in the vicinity of the higher edge of the Σ^- peak. The background is taken as a smooth curve whose slope changes quickly near this threshold, which yields the result

$$B(\psi\to\Lambda\bar{\Sigma}^+\pi^-)=(1.53\pm0.17\pm0.38)\times10^{-3}\ . \quad (56)$$

We now turn to the charge-symmetric mode and plot the missing mass opposite the $\Lambda\pi^+$ system, shown in Fig. 27(b). While the $\Lambda\pi^-$ can be the decay of a Ξ^-, here no such decay is present. There is good evidence for an enhancement on top of a combinatorial background, centered near 1.18 GeV/c^2, which we attribute to the decay

$$\psi\to\Lambda\bar{\Sigma}^-\pi^+\ . \quad (57)$$

The background is subtracted as above which leads to a branching ratio

$$B(\psi\to\Lambda\bar{\Sigma}^-\pi^+)=(1.38\pm0.21\pm0.35)\times10^{-3}\ . \quad (58)$$

We extend our three-body search to include heavier mesons opposite the $N\bar{N}$ system. Figure 28 shows the $m_m{}^2$ opposite two-prong $p\bar{p}$ events. There is a clear enhancement centered at $m_m{}^2=0.3$ (GeV/c^2)^2, which we attribute to the decay

$$\psi\to p\bar{p}\eta\ . \quad (59)$$

A fit is done in Fig. 28, shown as a solid curve, which yields the result

$$B(\psi\to p\bar{p}\eta)=(2.03\pm0.13\pm0.16)\times10^{-3}\ . \quad (60)$$

These events are kinematically fit to the event hypothesis $\psi\to p\bar{p}\eta$. For the 1101 events which have successful fits, we form the Dalitz plot for the events, shown in Fig. 29. The depopulations at high $p\eta$ mass are due to detector inefficiencies for soft protons. The Dalitz plot exhibits a highly nonuniform population which peaks at

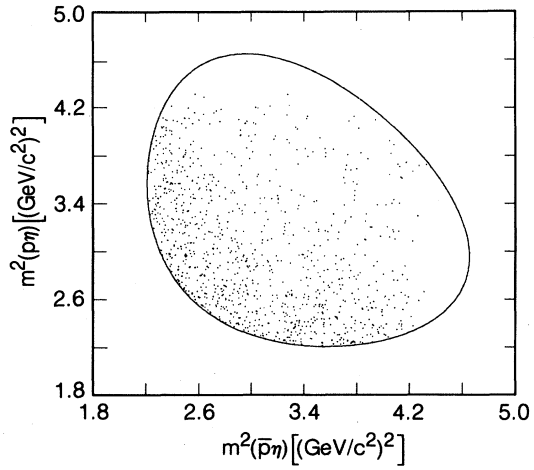

FIG. 29. Dalitz plot for $\psi\to p\bar{p}\eta$. The events in this plot have been kinematically constrained to the event hypothesis.

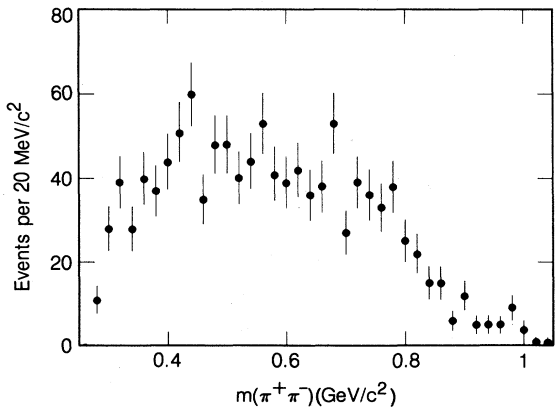

FIG. 31. $m(\pi^+\pi^-)$ in $\psi\to p\bar{p}\pi^+\pi^-$ events, where $\psi\to\Lambda\bar{\Lambda}$ and $\psi\to\Delta^{++}\Delta^{--}$ events have been removed. Note the absence of a ρ^0 enhancement.

low $p\eta$ mass, and is poorly described by phase space. This may be seen by plotting the $p\eta$ projections in Fig. 30. The projections tend to peak at $\simeq 2.52$ $(\mathrm{GeV}/c^2)^2$, but there is no clear evidence for resonance formation. The S'_{11} nucleon state $N(1535)$ has a substantial branching fraction ($\simeq 55\%$) into $N\eta$, and we may be seeing the influence of this resonance. Alternately, this effect may be interpreted as the dominance of one $p\bar{p}$ partial wave in the decay, leading to a broad enhancement near the maximum of the allowed $p\bar{p}$ mass.

Another three-body decay we consider is the reaction

$$\psi \to p\bar{p}\rho^0 . \tag{61}$$

This analysis naturally arises out of the results in Sec. X regarding the decay $\psi \to p\bar{p}\pi^+\pi^-$ (73), where the $\psi \to \Lambda\bar{\Lambda}$ and $\psi \to \Delta^{++}\bar{\Delta}^{--}$ events have been removed. Figure 31 shows the $\pi^+\pi^-$ mass plot for the remaining events. No evidence is seen for the decay (61). Attributing events in the region $0.71 < m(\pi^+\pi^-) < 0.79$ GeV/c^2 to reaction (61), we obtain a limit

$$B(\psi \to p\bar{p}\rho^0) < 0.31 \times 10^{-3} \tag{62}$$

at the 90% confidence level.

The decay

$$\psi \to p\bar{p}\omega , \tag{63}$$

however, is clearly present. Figure 32 shows the missing mass against the $p\bar{p}$ system, where now we allow more than two charged prongs in the event due to the ω decay modes. There is a clear enhancement centered near 0.78 GeV/c^2, which comes from reaction (63). We fit the missing-mass spectrum, and obtain

$$B(\psi \to p\bar{p}\omega) = (1.10 \pm 0.17 \pm 0.18) \times 10^{-3} . \tag{64}$$

The constrained Dalitz plot for reaction (63) has been investigated. No evidence for resonant behavior is found.

The decay

$$\psi \to p\bar{p}\eta' \tag{65}$$

is kinematically just allowed. Since the decay $\eta' \to \eta\pi\pi$ has a very small Q value, the η' is detected via its $\rho^0\gamma$ decay mode. The branching fraction of the η' to $\rho^0\gamma$ is much smaller than to $\eta\pi\pi$, but this is compensated by the increase in detection efficiency for the $\rho^0\gamma$ decay mode, where the γ is not observed. Figure 19 shows the quantity U versus the mass of four-prong $p\bar{p}\pi^+\pi^-$ events. There is a clear band of events centered near the bottom of Fig. 19, which is consistent with the decays

$$\psi \to p\bar{p}\pi^+\pi^-\gamma \tag{44}$$

and

$$\psi \to p\bar{p}\pi^+\pi^-\pi^0 . \tag{45}$$

As in the $\psi \to p\bar{p}\pi^0(\gamma)$ case, we cannot distinguish between (44) and (45) without photon detection. For events which fall in this band, we perform a one-constraint fit to the event hypothesis (44). For the 211 events of the four-prong mass < 3 GeV/c^2 with successful fits, we plot the $\pi^+\pi^-\gamma$ mass, shown in Fig. 33. There is a small but narrow enhancement centered at $\simeq 0.95$ GeV/c^2, which we attribute to reaction (65). Note that the γ from the η' decay is so soft that we cannot observe it in our apparatus, consistent with the result (46). Taking as the signal region the two bins centered at 0.945 and 0.955, we find

$$B(\psi \to p\bar{p}\eta') = (0.68 \pm 0.23 \pm 0.17) \times 10^{-3} . \tag{66}$$

Charged kaon production is observed in events contain-

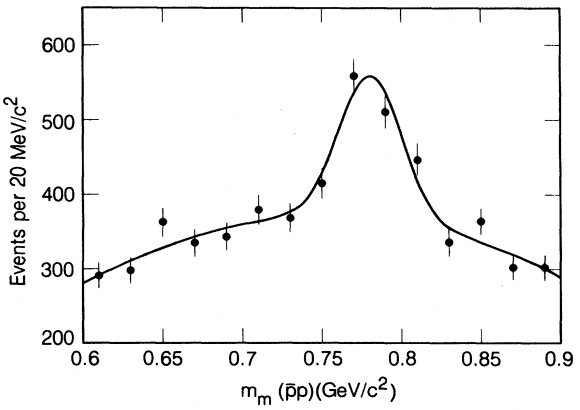

FIG. 32. Missing mass against inclusive $p\bar{p}$ pairs at the ψ. The peak near $0.78 = \mathrm{GeV}/c^2$ is from the decay $\psi \to p\bar{p}\omega$. Solid line is fit discussed in the text.

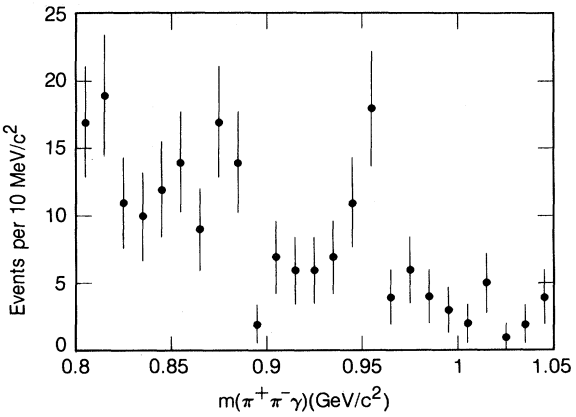

FIG. 33. $\pi^+\pi^-\gamma$ mass in $\psi \to p\bar{p}\pi^+\pi^-\gamma$ events. The peak near 0.96 GeV/c^2 is from the decay $\psi \to p\bar{p}\eta'$.

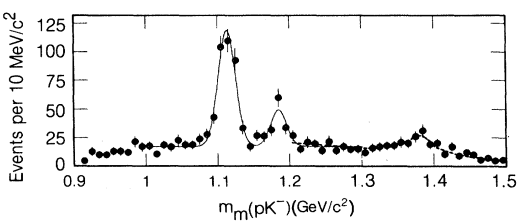

FIG. 34. Missing mass opposite pK^- and $\bar{p}K^+$ pairs combined. Note the resonant structure. The solid curve is from the simultaneous fit to $\psi \to p\bar{\Lambda}K^-$ and $\psi \to p\bar{\Sigma}^0K^-$, while the dashed curve is from the fit to $\psi \to p\bar{\Sigma}^0(1385)K^-$. Both fits are described in text.

ing baryons at the ψ. The missing mass for two-prong pK^- events is shown in Fig. 34. There are two clear peaks in the vicinity of 1.15 GeV/c^2. The first peak, centered near 1.115 GeV/c^2, we attribute to the decay

$$\psi \to \bar{p}\Lambda K^+ , \tag{67}$$

while the peak centered near 1.19 GeV/c^2 comes from the decay

$$\psi \to \bar{p}\Sigma^0 K^+ . \tag{68}$$

Due to the proximity of the Λ and the Σ^0 masses, we simultaneously fit the missing-mass spectrum of both peaks, shown as a solid line in Fig. 34. The simultaneous fit properly accounts for the background under the peaks, whence

$$B(\psi \to \bar{p}\Lambda K^+) = (0.89 \pm 0.07 \pm 0.14) \times 10^{-3} \tag{69}$$

and

$$B(\psi \to \bar{p}\Sigma^0 K^+) = (0.29 \pm 0.06 \pm 0.05) \times 10^{-3} . \tag{70}$$

We have also investigated the constrained Dalitz plot for events consistent with reaction (67). No evidence was found for any resonance formation.

There is also a broad but unmistakable peak centered near 1.38 Gev/c^2 in Fig. 34, which we attribute to the decay

$$\psi \to \bar{p}\Sigma^0(1385) K^+ . \tag{71}$$

The same data have been refitted to a Breit-Wigner form, shown as a dashed line in Fig. 34. This yields the result

$$B(\psi \to \bar{p}\Sigma^0(1385) K^+) = (0.51 \pm 0.26 \pm 0.18) \times 10^{-3} . \tag{72}$$

X. MULTIBODY DECAY MODES OF THE ψ

We now investigate decay modes of higher multiplicity. Multibody decay modes usually have large resonant contributions, which must be measured to determine the nonresonant contribution. We first discuss the decay

$$\psi \to p\bar{p}\pi^+\pi^- , \tag{73}$$

whose major background is the decay $\psi \to \Lambda\bar{\Lambda}$. We remove these events by making the Goldhaber plot for $p\pi^-$ combinations, and requiring all further events to lie outside a circle of radius 10 MeV/c^2 about the nominal $\Lambda\bar{\Lambda}$ mass point. For these events, we plot the mass of the $p\bar{p}\pi^+\pi^-$ system, as shown in Fig. 35. There is a clear excess of events centered at 3.1 GeV/c^2, which we attribute to reaction (73). We take as the signal region $3.05 < m(p\bar{p}\pi^+\pi^-) < 3.14$ GeV/c^2, which yields the result

$$B(\psi \to p\bar{p}\pi^+\pi^-) = (6.46 \pm 0.17 \pm 0.43) \times 10^{-3} . \tag{74}$$

The summed $p\pi^+$ projections for reaction (73) have been plotted in Fig. 12. The solid histogram corresponds to a Monte Carlo phase-space calculation normalized to the same number of events as the data. Taking the signal region as $1.18 < m(p\pi^+) < 1.32$, and using phase space as an estimate of the background, the number of $p\pi^+$ combinations originating from Δ^{++} decays is 678±39 pairs. Note that events from the decay $\psi \to \Delta^{++}\bar{\Delta}^{--}$ (26) will be counted twice in this plot. The fraction of time f, a $p\pi^+$ pair will be resonant as a Δ^{++} is

$$f(p\pi^+ \text{ as } \Delta^{++}) = 0.195 \pm 0.030 \pm 0.049 . \tag{75}$$

Much of the Δ^{++} production comes from reaction (26), discussed in Sec. VII, while the residual production comes from the decay $\psi \to \Delta^{++}\bar{p}\pi^-$ (53).

The $\Delta^{++}\bar{\Delta}^{--}$ region, as defined in Sec. VI, is removed from further analysis. We now return our attention to the $p\pi^-$ system. Shown in Fig. 36 is the invariant mass of the $p\pi^-$ combinations. There is a slight excess of 78±22 events, centered near 1.22 GeV/c^2, which we attribute to the neutral P_{33} resonance the Δ^0. Correcting for the $\Delta^{++}\bar{\Delta}^{--}$ region subtracted out which reflects into the $p\pi^-$ signal region, we can quote the fraction of the time, f, that the $p\pi^-$ system is in a Δ^0:

$$f(p\pi^- \text{ as } \Delta^0) = 0.029 \pm 0.008 \pm 0.007 . \tag{76}$$

Since the ψ is an isoscalar, all four of the $I = \frac{3}{2}$ isospin states should be evenly populated. Consequently, the frac-

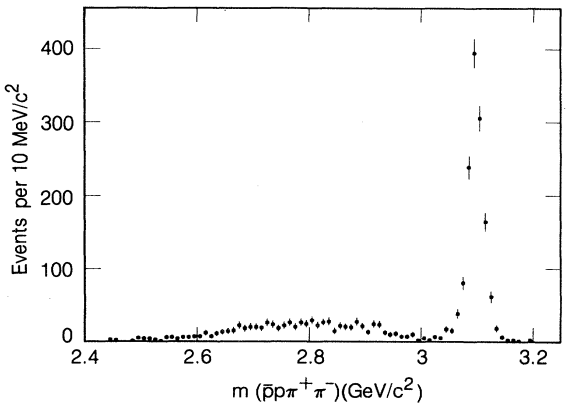

FIG. 35. Mass plot for four-prong $p\bar{p}\pi^+\pi^-$ events, where events with both neutral $p\pi$ combinations having the Λ mass have been removed. The peak near 3.1 GeV/c^2 is due to the decay $\psi \to p\bar{p}\pi^+\pi^-$.

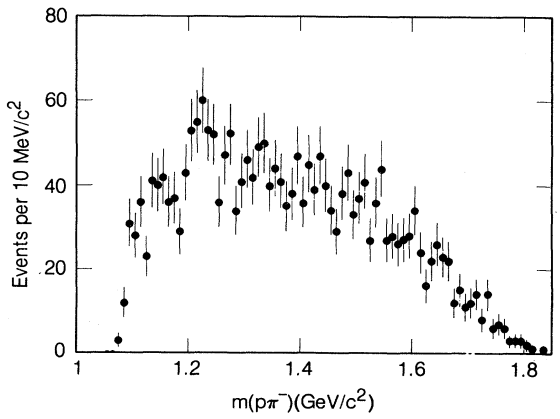

FIG. 36. $m(p\pi^-)$, where $\psi \to \Lambda\bar{\Lambda}$ and $\psi \to \Delta^{++}\bar{\Delta}^{--}$ events have been subtracted. The slight enhancement near 1.23 GeV/c^2 is from the decay $\Delta^0 \to p\pi^-$.

tion of Δ^{++} pairs should be nine times that of the Δ^0 pairs, as the Δ^0 decays to $p\pi^-$ only one third of the time. The ratio is

$$\frac{f(p\pi^+ \text{ as } \Delta^{++})}{f(p\pi^- \text{ as } \Delta^0)} = 6.7 \pm 3.2 \,, \tag{77}$$

consistent with isospin conservation.

We now discuss the reaction

$$\psi \to p\bar{p}\pi^+\pi^-\pi^0 \,. \tag{45}$$

From the null result for the reaction $\psi \to p\bar{p}\pi^+\pi^-\gamma$ (44) obtained in Sec. IX, we attribute essentially all events in the band centered near $U=0$ to reaction (45). The quantity U is shown in Fig. 37 for all events with $m(p\bar{p}\pi^+\pi^-) < 3$ GeV/c^2. Included are contributions from $\psi \to p\bar{p}\omega$ (63) and $\psi \to p\bar{p}\eta$ (59). Figure 38 shows the missing mass against the $p\bar{p}$ system for these events, where the events have been constrained to the event hypothesis (45) to improve mass resolution. The contributions from the decays (63) and (59) are clearly visible. These resonant contributions have been calculated and agree well with the previous calculations. A subtraction of these contributions yields the result

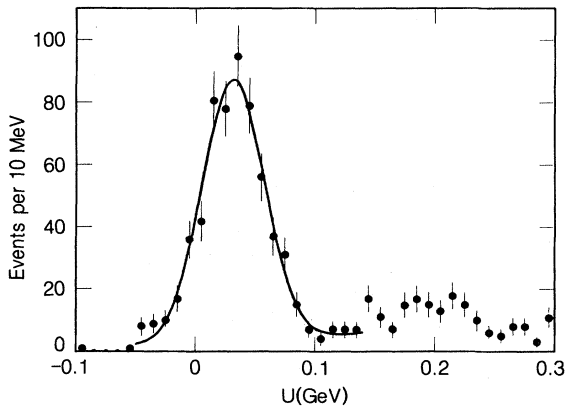

FIG. 37. The quantity U for all $p\bar{p}\pi^+\pi^-$ events. The peak near $U=0$ is from the decays $\psi \to p\bar{p}\pi^+\pi^-\gamma(\pi^0)$. Solid curve is fit described in text.

$$B(\psi \to p\bar{p}\pi^+\pi^-\pi^0) = (3.36 \pm 0.65 \pm 0.28) \times 10^{-3} \,. \tag{78}$$

TABLE VI. Summary of ψ decay modes (units of 10^{-3}).

Decay mode[a]	Events	ϵ	B for this experiment	Mark I (Ref. 31) (±15% systematic errors)
$\psi \to p\bar{p}$	1420±37	0.497	2.16±0.07±0.15 (8)	2.2 ±0.2
$\psi \to \Lambda\bar{\Lambda}$	365±19	0.176	1.58±0.08±0.19 (11)	1.1±0.2
$\psi \to \Sigma^0\bar{\Sigma}^0$	90±9	0.043	1.58±0.16±0.25 (17)	1.3±0.4
$\psi \to \Xi^-\bar{\Xi}^+$	194±14	0.129	1.14±0.08±0.20 (22)	1.4±0.5
$\psi \to \Delta^{++}\bar{\Delta}^{--}$	233±19	0.160	1.10±0.09±0.28 (27)	
$\psi \to \Sigma^-(1385)\bar{\Sigma}^+(1385)$	56±14	0.050	0.86±0.18±0.22 (29)	
$\psi \to \Sigma^+(1385)\bar{\Sigma}^-(1385)$	68±16	0.050	1.03±0.24±0.25 (31)	
$\psi \to \Sigma^-(1385)\bar{\Sigma}^+$	26±10	0.067	0.29±0.11±0.10 (34)	
$\psi \to \Sigma^+(1385)\bar{\Sigma}^-$	28±10	0.068	0.31±0.11±0.11 (36)	
$\psi \to p\bar{p}\gamma$	49±9	0.195	0.38±0.07±0.07 (42)	<0.11
$\psi \to p\bar{p}\pi^+\pi^-\gamma$	<12	0.023	<0.79 (46)	
$\psi \to p\bar{p}\pi^0$	685±56	0.458	1.13±0.09±0.09 (47)	1.00±0.15
$\psi \to p\bar{n}\pi^-$ [incl. $p\bar{N}^-(1440-1535)$]	1288±47	0.482	2.02±0.07±0.16 (49)[a]	2.16±0.29
$\psi \to \bar{p}n\pi^+$ [incl. $\bar{p}N^+(1440-1535)$]	1191±47	0.467	1.93±0.07±0.16 (50)[a]	2.04±0.27
$\psi \to \bar{p}N^+(1440-1535)$	189±31	0.153	0.93±0.15±0.32 (52)	
$\psi \to \Delta^{++}\bar{p}\pi^-$	332±49	0.159	1.58±0.23±0.40 (54)	
$\psi \to \Lambda\bar{\Sigma}^+\pi^-$ [incl. $\Sigma^-(1385)\bar{\Sigma}^+$]	135±15	0.067	1.53±0.17±0.38 (56)	
$\psi \to \Lambda\bar{\Sigma}^-\pi^+$ [incl. $\Sigma^+(1385)\bar{\Sigma}^-$]	118±18	0.065	1.38±0.21±0.35 (58)	
$\psi \to p\bar{p}\eta$	826±52	0.309	2.03±0.13±0.15 (60)	2.3±0.4
$\psi \to p\bar{p}\rho^0$	38±16	0.158	<0.31 (62)	
$\psi \to p\bar{p}\omega$	486±73	0.323	1.10±0.17±0.18 (64)	1.6±0.3
$\psi \to p\bar{p}\eta'$	19±6	0.021	0.68±0.23±0.17 (66)	1.8±0.6
$\psi \to pK^-\bar{\Lambda}$	307±25	0.262	0.89±0.07±0.14 (69)	
$\psi \to pK^-\bar{\Sigma}^0$	90±19	0.236	0.29±0.06±0.05 (70)	
$\psi \to pK^-\bar{\Sigma}^0(1385)$	89±46	0.132	0.51±0.26±0.18 (72)	
$\psi \to p\bar{p}\pi^+\pi^-$ (incl. $\Delta^{++}\bar{\Delta}^{--}$ and $\Delta^{++}\bar{p}\pi^-$)	1435±38	0.168	6.46±0.17±0.43 (74)	5.5±0.6
$\psi \to p\bar{p}\pi^+\pi^-\pi^0$	364±70	0.082	3.36±0.65±0.28 (78)	1.6±0.6

[a]For those cases in which the final states and their charge conjugates are not the same, both are included in the quoted numbers with the exception of reactions (49) and (50) for which each charge-conjugate state is quoted separately.

XI. SUMMARY AND CONCLUSIONS

Table VI summarizes the measurements made by this experiment. A comparison to those previously reported by the Mark I experiment is also given. A substantial number of new decay modes have been measured, while the results of this experiment are in good agreement with those of the Mark I experiment.

This experiment has measured a number of two-body decay modes of the ψ, which allow a detailed test to the $SU(3)_f$ structure of the ψ. The results of Secs. V and VI regarding the decays $\psi \to B_8 \bar{B}_8$ (24) and $\psi \to B_{10} \bar{B}_{10}$ (32) are totally compatible with the ψ being a pure $SU(3)_f$ singlet. However, the results of Sec. VII on the decays $\psi \to B_8 \bar{B}_{10}$ (37) give within the limited statistics the first indication of a substantial branching ratio for a $SU(3)_f$-forbidden decay. It seems surprising that the $SU(3)_f$-forbidden amplitude in Sec. VII does not appear to influence the results of Secs. V and VI.

The exclusive radiative decay $\psi \to p\bar{p}\gamma$ (38) has been observed with a rate relative to the decay $\psi \to p\bar{p}$ (5) comparable with that of the first-order inclusive QCD prediction. This experiment is not sensitive enough to observe any other exclusive direct-photon decays involving baryons. There is no conclusive evidence for a bound state opposite the direct photon, although a broad enhancement near threshold is observed in events consistent with the decays $\psi \to p\bar{p}\gamma$ (38) and $\psi \to p\bar{p}\pi^0$ (40).

We have presented in Sec. IX measurements of a large variety of three-body decay modes of the ψ, nearly all of which have branching ratios of order 1×10^{-3}. The exception is the decay $\psi \to p\bar{p}\rho^0$, which appears suppressed. This is particularly interesting in that the decay $\psi \to p\bar{p}\omega$ (63) is not suppressed relative to the other allowed three-body states. Included in these measurements are several charge-symmetric modes. These measurements are totally consistent with the ψ being an isoscalar. Substantial resonance formation is observed in three-or-more-body decay modes of the ψ. Both Δ^{++} and Δ^0 production are observed in the decay $\psi \to p\bar{p}\pi^+\pi^-$, at rates again consistent with the ψ being an isoscalar.

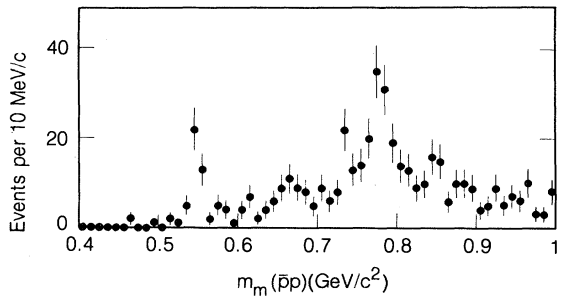

FIG. 38. Missing mass opposite the $p\bar{p}$ system for $\psi \to p\bar{p}\pi^+\pi^-\pi^0(\gamma)$ events. The events in this figure have been constrained to the hypothesis $\psi \to p\bar{p}\pi^+\pi^-\pi^0$. The peaks near 0.55 and 0.78 GeV/c^2 are due to the decays $\psi \to p\bar{p}\eta$ and $\psi \to p\bar{p}\omega$, respectively.

ACKNOWLEDGMENTS

We thank M. Suzuki and R. Cahn for helpful discussions. This work was supported primarily by the U. S. Department of Energy under Contracts Nos. DE-AC03-76SF00515 and DE-AC03-76SF00098. Support for individuals came from listed institutions plus Der Deutsche Akademische Austauschdienst, Bonn, Germany (M.T.). The Miller Institute for Basic Research in Science, Berkeley, California (G.H.T.), Ecole Polytechnique, Paliseau, France (I.V.), and Centre d' Etudes Nucleaires de Saclay, France (H.Z.).

[a]Present address: Harvard University, Cambridge, MA 02138.
[b]Present address: Carnegie-Mellon University, Pittsburgh, PA 15213.
[c]Present address: DESY, Hamburg, Federal Republic of Germany.
[d]Present address: XEROX Corporation, Palo Alto, CA.
[e]Present address: Fermilab, Batavia, IL 60510
[f]Present address: University of Massachusetts, Amherst, MA 01003.
[g]Present address: CERN, CH-1211 Geneva 23, Switzerland.
[h]Present address: LPNHE, Ecole Polytechnique, F-91128 Palaiseau, France.
[i]Present address: Vanderbilt University, Nashville, TN 37235.
[j]Present address: California Institute of Technology, Pasadena, CA 91125.
[k]Present address: CEN Saclay, F-91190 Gif-sur-Yvette, France.
[l]Present address: Techn. Hochschule Aachen, Federal Republic of Germany.
[m]Present address: Argonne National Laboratory, Argonne, IL 60439.

[1]L. B. Okun and M. B. Voloshin, Institute of Theoretical and Experimental Physics, Moscow, Report No. ITEP-95-1976, 1976 (unpublished).
[2]S. J. Brodsky, T. A. DeGrand, R. R. Horgan, and D. G. Coyne, Phys. Lett. 73B, 203 (1978).
[3]K. Koller and T. Walsh, Nucl. Phys. B140, 449 (1978).
[4]W. Bartel *et al.*, Phys. Lett. 64B, 483 (1976).
[5]W. Bartel *et al.*, Phys. Lett. 66B, 489 (1977).
[6]W. Braunschweig *et al.*, Phys. Lett. 67B, 243 (1977).
[7]G. Alexander *et al.*, Phys. Lett. 72B, 493 (1978).
[8]R. Brandelik *et al.*, Phys. Lett. 74B, 292 (1978).
[9]D. L. Scharre, in *Current Hadron Interactions, Vol. II* of Proceedings of the XIV Rencontre de Moriond, Les Arcs, France, 1979, edited by J. Trân Thanh Vân (Editions Frontières, Dreux, France, 1979), p. 219.
[10]R. Partridge *et al.*, Phys. Rev. Lett. 44, 712 (1980).
[11]D. L. Scharre *et al.*, Phys. Lett. 97B, 329 (1980).
[12]C. Edwards *et al.*, Phys. Rev. Lett. 48, 458 (1982).
[13]T. Appelquist, A. De Rújula, H. D. Politzer, and S. L. Glashow, Phys. Rev. Lett. 34, 365 (1975).
[14]M. S. Chanowitz, Phys. Rev. D 12, 918 (1975).
[15]G. S. Abrams *et al.*, Phys. Rev. Lett. 44, 114 (1980).
[16]D. L. Scharre *et al.*, Phys. Rev. D 23, 43 (1981).

[17]M. T. Ronan *et al.*, Phys. Rev. Lett. 44, 367 (1980).
[18]We use the notation B_8 to denote any member of the lowest-lying $\frac{1}{2}^+$ baryon octet, and B_{10} to denote any member of the lowest-lying $\frac{3}{2}^+$ baryon decuplet.
[19]Unless explicitly mentioned, the charge-conjugate reaction is always implied.
[20]G. S. Abrams *et al.*, Phys. Rev. Lett. 43, 477 (1979).
[21]H. Brafman *et al.*, IEEE Trans. Nucl. Sci. NS25, 692 (1978).
[22]T. M. Himel, Ph.D. thesis, Stanford University, SLAC Report No. 223, 1979.
[23]G. S. Abrams *et al.*, Phys. Rev. Lett. 44, 10 (1980).
[24]R. H. Schindler *et al.*, Phys. Rev. D 24, 78 (1981).
[25]M. W. Eaton, Ph.D. thesis, University of California, Report No. LBL 14581, 1982.
[26]As will be seen in the following sections, there is no evidence for any isospin violation in the decay modes of the ψ including baryons.
[27]This is of course an approximation as we have completely ignored any momentum dependence that the matrix element might have.
[28]S. J. Brodsky and G. P. Lepage, Phys. Rev. D 24, 2848 (1981).
[29]M. Claudson, S. L. Glashow, and M. B. Wise, Phys. Rev. D 25, 1345 (1982).
[30]T. Himel *et al.*, Phys. Rev. Lett. 45, 1146 (1980).
[31]I. Peruzzi *et al.*, Phys. Rev. D 17, 2901 (1978).
[32]Note that the photon from the decay $\psi \to p\bar{p}\eta'$ where the η' decays to $\rho^0\gamma$ is so soft as to be undetectable, and as such does not show up here.